Agglomeration in counter-current spray drying towers. Part B: Interaction between multiple spraying levels

Francia Garcia, Victor; Martin, Luis; Bayly, Andrew E.; Simmons, Mark J.h.

DOI:
10.1016/j.powtec.2016.05.010

Powder Technology xxx (2016) xxx–xxx

Contents lists available at ScienceDirect

Powder Technology

journal homepage: www.elsevier.com/locate/powtec

Agglomeration in counter-current spray drying towers. Part B: Interaction between multiple spraying levels

Víctor Francia [a,b,*], Luis Martín [b], Andrew E. Bayly [b,1], Mark J.H. Simmons [a]

[a] School of Chemical Engineering, University of Birmingham, Birmingham,B15 2TT,United Kingdom
[b] Procter & Gamble, R & D, Newcastle Innovation Centre, Newcastle upon Tyne, United Kingdom

ARTICLE INFO

Article history:
Received 20 November 2015
Received in revised form 6 May 2016
Accepted 7 May 2016
Available online xxxx

Keywords:
Spray drying
Agglomeration
Aggregation
Coalescence
Spray
Nozzle

ABSTRACT

A new experimental method is developed here to investigate agglomeration in spray drying towers operating with multiple nozzles. It allows studying independently the contribution of each spray to the product and obtaining a valuable insight into the agglomeration processes. The paper studies a two level swirl counter-current dryer of detergent in a full-scale production system. It shows that operation with two nozzle levels increases the energy efficiency compared to the use of single sprays, but in turn promotes both agglomeration and elutriation of powder from the top of the dryer. The product size distribution becomes bi-modal and the composition and porosity of the product more heterogeneous due to the different thermal histories experienced by droplets from each spray. The method described here controls the air temperature and humidity nearby the nozzles to quantify the agglomerates resulting from particle contacts within each individual spray or from their interaction. Particle agglomeration is shown to be suppressed at the bottom of the dryer where the heat transfer rates are highest and promoted at the top spray, which originates a second coarse mode in the size distribution. Both levels do not operate independently; the powder elutriated upwards from the bottom nozzle is captured entirely by the top spray when it is centrally located. By isolating the independent impact of each nozzle in a dryer, the method provides powerful data to correlate the agglomeration behaviour with local process conditions, and so facilitate the development and validation of spray dryer models.

1. Introduction

Spray dryers are used for obtaining particulate products from stocks of materials with high humidity. Slurries or pastes are atomised in a drying chamber and the contact with hot air removes the moisture, turning the droplets into porous particles. Advantages versus other alternatives include the ability to encapsulate active components in a solid matrix and obtaining fast dissolving powders with an open structure, which is often desirable for consumer goods [1]. Thermally stable products are spray dried in counter-current devices to minimise the consumption of energy. In turn, the counter flow accumulates solids and causes more agglomeration, breakage and deposition than a co-current device. Detergent powders can be manufactured in this way, making use of large towers and a strong swirl to increase the relative velocity between the phases [2,3]. The swirl makes the solids to concentrate close to the walls, where they form multi-layered deposits [4] that interact with air borne powder through the deposition of new material and re-entrainment of clusters back into the flow. The deposition/resuspension cycle then gives rise to substantial agglomeration and much of the residence time experienced by the solids [5].

The design and scale up of dryers still needs to rely on experience [6,7]. The flow dynamics depends on an intimate coupling between both phases [8–10] and it is often impossible to describe without a certain knowledge of how the solids come into contact, grow [11,12] or deposit [13–15]. The change in size affects drastically the way the particles disperse, particularly under swirl [16,17]; it determines the quality of the powder and the rate of heat and mass transfer [18–20]. Stochastic models [21] allow for tracking particle-particle impacts and introducing growth models [22–25] but significant research is needed to describe accurately the contact between semi-dried particles [26,27]. It is generally accepted that comprehensive tools are still far from capturing agglomeration phenomena [28,29] particularly in counter-current towers where the number of contacts is exacerbated. Swirl towers have been adapted to different formulations over decades to maximise capacity and efficiency [3], both of which depend on the evolution of the particle size. In essence, the rate of a dryer is limited by the amount of slurry that can be dried without causing excessively coarse or fine particles. Agglomeration in a swirl tower becomes more important when one operates at a high throughput, for instance by placing more sprays in the chamber [30–32]. Ultimately, the powder becomes too

* Corresponding author.
E-mail address: v.francia.chemeng@gmail.com (V. Francia).
[1] Present address: *School Chemical and Process Engineering, University of Leeds, Leeds, UK.*

http://dx.doi.org/10.1016/j.powtec.2016.05.010

coarse and wet, and the fraction that must be discarded turns too high. Research has focused on the air fluid dynamics [33,34], but experimentation in full scale (e.g. >100-1000 m^3) is challenging and obtaining reliable data is complicated [35]. In manufacturing scales, residence times were first reported by Place [36], but more recently, stability analysis [37], velocity [38] and flow and turbulence data have become available [39]. As a consequence of a limited experimentation it has not been possible to validate the few multi-phase models available [40–43], which rely on data in laboratories [33] or pilot scale facilities [34] and very rarely deal with the solid phase [44–46], particle contacts [47] or deposits. Only few authors such as Fieg [48] or Zbiciński [40] study experimentally the properties of the solids and report temperatures or drying rates in pilot towers, but to our knowledge no full scale experimentation has linked agglomeration to process conditions, nozzle configuration or energy efficiency.

To this purpose, two independent investigations have been conducted. Part A [49] compartmentalises a swirl drying tower and documents the use of single detergent nozzles; it clarifies the effects arising from the separation of solid and liquid phases during the atomization and correlates the location of a nozzle to the capacity and efficiency of the dryer. The nozzle position can be manipulated to minimise elutriation and control growth [49], but to maximise throughput, the largest units introduce various nozzles levels [30–32]. Further research is needed to understand the role of the nozzle configuration: where and how the aggregates are formed, how the drying efficiency changes from using one to various levels or whether the different sprays interact. This paper, Part B, answers some of these questions studying the transition from a single-level operation to the use of two spraying levels with central nozzles. The experimental method developed here allows studying, for the first time, the contribution of each nozzle to the product, quantifying the interaction between sprays and correlating the local conditions to experimental growth patterns. This type of data enables the simplification of models to the areas in a dryer where agglomeration is most relevant.

2. Experimental conditions

2.1. Unit design and measurement

An industrial counter-current spray drying tower was used for the experiments, property of Procter & Gamble. Table 1 includes the main design features and Fig. 1 depicts the location of slurry and water nozzles. Fig. 2 illustrates the operation of the air system, the location of temperature sensors and wall inspection areas.

The hot air is injected at the bottom of the dryer with certain angular momentum. A vortex is formed at the conical section [39]; it moves into the cylinder and exits through the top duct entering a series of cyclones, where the powder elutriated from the chamber is collected. The same formulation and atomization conditions used in Part A [49] and other works [5] are maintained. The paste is prepared by the addition of surfactant(s), polymer(s) and inorganic salt(s) up to a solid content between 30-60% It is pressurised and conducted into swirl pressure nozzles at positions #1 and #3 in Fig. 1, where it is atomized. The same nozzle is used at all levels, aligned with the centreline of the chamber and facing down. Droplets sufficiently light are entrained in the upwards air flow. Some exit the tower top and are collected at the cyclones and those sufficiently coarse migrate to the wall before reaching the top exit, concentrate, grow and start to flow down. Intermediate droplet sizes move outwards from the spray and approach the terminal velocity before reaching the wall above or below the nozzle. Increasing in size,

Table 1
Tower design parameters.

d/D	H/D	$^{*}\Omega_i$
0.29	10.58	5.1 - 5.4

* Ω_i *initial swirl intensity* [39]

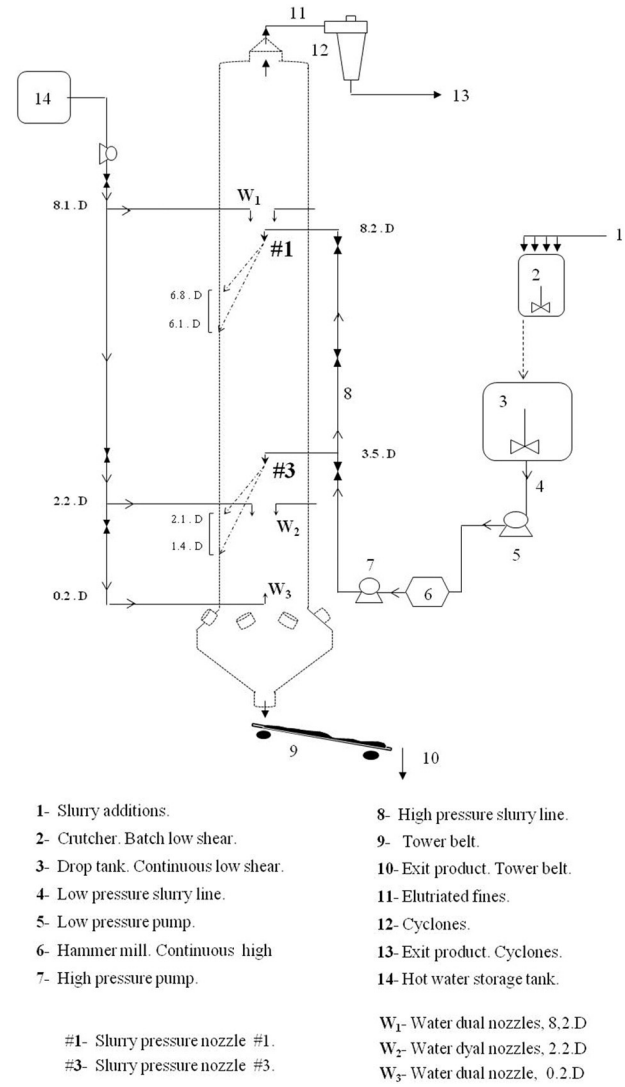

Fig. 1. Description of the counter-current dryer, the water and the slurry lines and nozzles. The projection of the slurry nozzles onto the walls depicts the thickness of a hollow cone spray.

droplets become less affected by drag and maintain a high momentum when they impact the wall for the first time. Fig. 1 depicts the area of the projection of the spray based in the spraying angle and the thickness of the hollow cone formed. Once the solids are dispersed near the wall, they free fall maintaining the swirling motion and collide multiple times with the structure of deposits formed.

The experiments described later make use of a fine water mist to control the air temperature and humidity in the chamber. To this effect, three sets of air atomized spray nozzles, denoted W_1, W_2 and W_3 (SU82, Fluid Cap 251376; Air Cap 4691312) were installed at the positions shown in Fig. 1, and fed from storage.

The air temperature T_A was measured automatically at the inlet, tt-0, and exhaust lines, tt-5 (Fig. 2). Any indication of the temperature inside the dryer is extremely valuable because it is rarely available and difficult to obtain [35]. In the chamber, measurements of air temperature T_A were obtained at four levels (tt-1 to tt-4, Fig. 1) placing hollow metallic bars with seven rectangular openings that expose K-type naked thermocouples to the flow. In agreement to Huntington [3], deposition and condensation in the sensors could be prevented by placing the bars sufficiently far from the sprays and aligning the openings in the shadow of the swirl. Comparison of this method to the exhaust probe results in good agreement (± 2 °C) in the absence of particles and similar humidity ranges. The evolution of the heat losses Q_{Loss} was

Please cite this article as: V. Francia, et al., Agglomeration in counter-current spray drying towers. Part B: Interaction between multiple spraying levels, Powder Technol. (2016), http://dx.doi.org/10.1016/j.powtec.2016.05.010

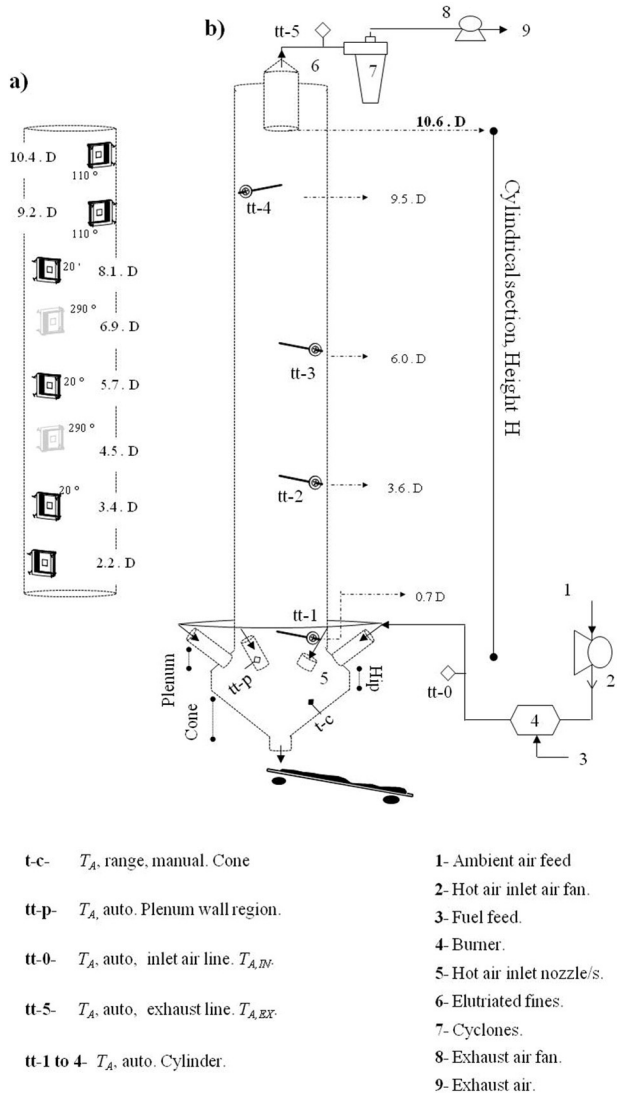

Fig. 2. (a) Inspection areas on the walls and (b) description of the hot air system and location of temperature sensors.

monitored by measurement of the wall temperature T_w at the conical section of the dryer.

Wall deposits grow during a long period until achieving a steady state thickness where deposition and re-entrainment become balanced [5]. The deposition rate in an initial stage $r_{d,o}$ is a good indication of the rate of impacts to the wall and often used for model validation. In line with usual practice [50,51] the initial deposition rate was measured at several locations (Fig. 2) by collection of the deposits formed over clean surfaces during 10-15 *min*.

The droplet size and the spray angle were obtained in an external spray rig with image analysis and laser diffraction methods (Malvern Spraytec Particle Sizer, RTSizer 5.6) respectively. The reader is referred to Part A [49] for a detailed study of atomization and the effects arising from the separation of solid and liquid phases at the nozzle.

The elutriation rate from the top of the chamber is measured by collection of the powder exiting the cyclones, later used for analysis. Ten 1 *kg* samples of the product exiting the bottom end were taken at the tower belt (Fig. 1) by collection of the full stream; they were sampled down and sieved using the Taylor series. The product temperature was measured by an infrared probe (OMEGA OS551). A larger bulk sample between 15-20 *kg* was also gathered by blending consecutive samples; it was sieved into 11 size fractions (Russell Finex Model 17240), sealed and used for analysis of composition, density and porosity. Water and surfactant(s) contents, X_w and X_s, were obtained with Toledo Mettler Moisture Balances and performing analytical titrations. Morphology was examined under Scanning Electron Microscopy, SEM, (Hitachi TM1000). Particle absolute, ρ_{abs}, and envelop,ρ_{env}, densities were analysed under He picometry (Micromeritics, AccuPyc II 1340 v1.02.01) and Hg Porosimetry (Micrometricts, Autopore IV) respectively.

2.2. Multi-level swirl dryers: Powder recirculation and drying kinetics

The capacity of a dryer is given by its ability to dry the maximum amount of product while controlling its properties, mainly size and density. Swirl dryers can distribute several nozzles in two or three rings at different levels [31,32] to maximise rate while minimising the number of particle contacts. Neighbouring sprays in each level can interact when they are too close to each other [3]. That effect is left out of the scope of this work, which focuses only on the transition from one to two levels of a single central nozzle. In this scenario, the introduction of a second nozzle level increases the production rate and modifies the dispersion and thermal history of the solid phase because (a) the inlet air mass rate and temperature need to be increased to convey more heat and mass transfer, (b) particles are injected at different places and so they present different residence times and (c) each spray faces different local temperatures and velocities.

Fig. 3 depicts the initial trajectory of different sized droplets and the subdivision of the dryer for a multi-level system. Part A [49] discusses in more detail this compartmentalization. One can focus in a concentrated ring close to the wall where the powder concentrates [4]. Regions above and below the spray(s) projection, denoted *SR*, *TR*, *ER* in Fig. 3 are defined as the areas where the particle motion is function of particle size and density but history independent. The nozzle region *NR* in turn is divided into (a) the spray (nozzle inertial region, *NIR* Fig. 3), which is comprised of high velocity droplets whose motion is dominated by the initial momentum and thus history, and (b) a concentrated area near the wall (nozzle terminal region, *NTR* Fig. 3) where free falling powder is exposed to high velocity droplets coming from the spray. In the nozzle region, the deposits need to be considered as a separate region, where wall-borne clusters interact with air-borne powder by rates of deposition and re-entrainment [5]. The transition from the single-level arrangement described in Part A to using two levels promotes agglomeration in three ways:

- **Collision rate or frequency:** The rate of particle-particle and particle-wall impacts increases in response to a higher concentration of solids. As the throughput is doubled it is necessary to convey more heat transfer in the dryer, which can be done by increasing the inlet air temperature and/or mass rate, $T_{A,IN}$ and M_A. As a result, the chamber develops higher air velocities U_A, which hold up more solids and elutriate more powder.

- **Probability of growth or collision efficiency:** The injection of the slurry at two different levels modifies the air temperature and velocity field, and so the droplets sprayed at each nozzle face different thermal histories. The largest driving force to dry the powder is generated at the bottom, where the air temperature T_A and velocity U_A are the highest. The surface of a droplet sprayed here must experience faster drying rates; it dries and turns non-deformable more rapidly, which reduces the likelihood for contacts to result in agglomeration or deposits. In contrast, droplets sprayed at the top face cooler and damper air and must remain prone to agglomerate or deposit for longer.

- **Recirculation and contact mechanics:** A characteristic feature of a multi-level configuration is the flow established between several nozzle regions. In this case, the product can be thought to be comprised of three different populations, p-i and p-ii: particles that come from each of the sprays without having aggregated or having done so with

Please cite this article as: V. Francia, et al., Agglomeration in counter-current spray drying towers. Part B: Interaction between multiple spraying levels, Powder Technol. (2016), http://dx.doi.org/10.1016/j.powtec.2016.05.010

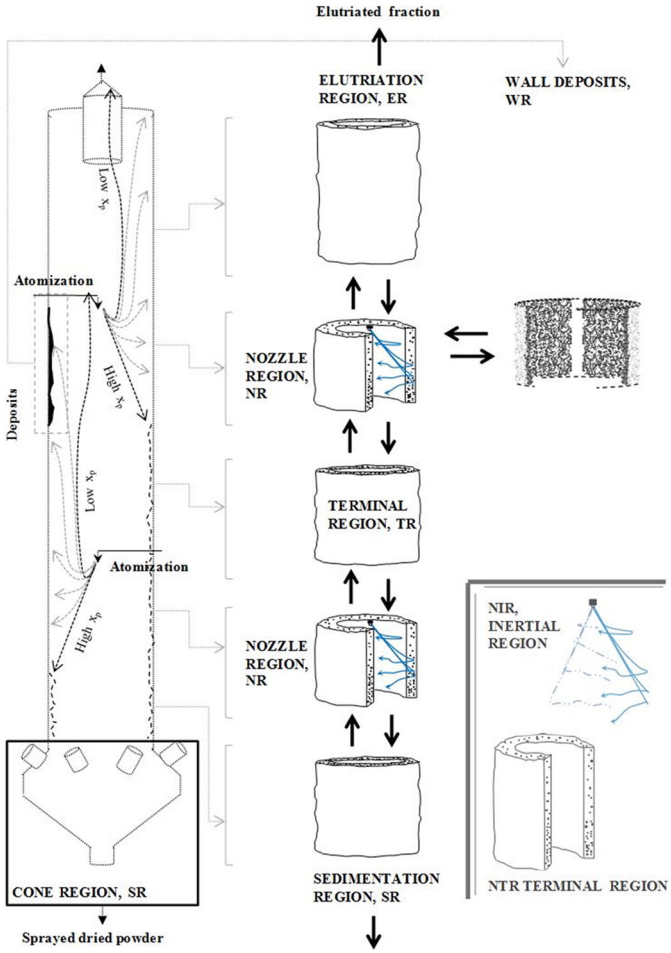

Fig. 3. Compartmentalization of a swirl counter-current dryer with two levels with central nozzles. Nozzle regions, *NR*, comprised of terminal *NTR* and inertial *NIR* regions; terminal *TR* sedimentation *SR* and elutriation *ER* regions and the cone region *CR*.

others from the same nozzle (e.g. coalescence near each *NIR* in Fig. 3), but also a different population p-iii: granules produced when the droplets/particles injected at different nozzles come into contact and aggregate. The contacts between particles from different sprays are likely to occur near each of the nozzle region(s), Fig. 4:

- **Top (NR #1):** Most of the powder elutriated from the bottom nozzle approaches the top spray near the walls in *NTR*. The finest drops however do not migrate outwards and reach the top at central positions within *NIR*, Fig. 4a. Here they face collision with high velocity droplets coming from the spray, which acts as a scrubber.

- **Bottom (NR #3):** The product from the top flows down near the wall and crosses the bottom spray *NIR* in Fig. 4b. These contacts occur in the concentrated annulus near the wall, *NTR* in Fig. 3. Here the solids stagnate, collide one to another and interact with high velocity drops coming from the bottom spray. The contacts with the particles coming from the top nozzle are no different to the rest of the powder in this region; they simply include solids that have had a longer residence time, and probably have already agglomerated in the top region.

The aim of this paper is to quantify the growth occurring in each of the nozzle regions shown in Fig. 3, and due to the recirculation flows depicted in Fig. 4.

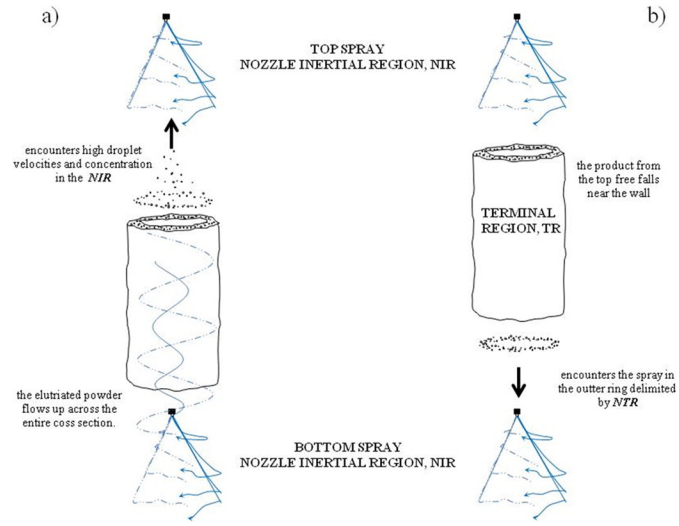

Fig. 4. Source of interactions between two nozzle regions *NRs* (a) the flux into the top nozzle region across the full cross-section i.e. *NIR* + *NTR* and (b) the flux from into the bottom nozzle region at the outer ring, *NTR*.

2.3. Experimental design

When one places a second nozzle level, it is complicated to distinguish the effects due to increasing the rate and the concentration of solids in the chamber or due to modifying the thermal history of each spray. The series of experiments outlined in Fig. 5 does so by studying each spray independently keeping a constant atomization. Three stages are followed:

1. **Reference.** The case M_{13} uses both slurry nozzles simultaneously and is taken as the reference.

2. **Isolation of each spray.** The top slurry nozzle in studied independently in M_1; the bottom in M_3, $M_{3\text{-ii}}$ and $M_{3\text{-iii}}$ using different levels of added water to control the air temperature and humidity within the nozzle region.

3. **Sensitivity**. The effect of reducing the inlet air temperature $T_{A,IN}$ and velocity U_A are studied in $M_{3\text{-i}}$.

During the start-up of M_{13} the hot air is connected; the inlet air temperature, $T_{A,IN}$ and rate, M_A are increased to heat up the dryer. When atomization starts, $T_{A,IN}$ is fixed and M_A increased until the product exits with the target water content X_w and the dryer wall reaches a constant temperature. The inlet conditions in M_{13} are used as the reference for the remaining experiments.

The isolation experiments try to identify which part of the product in M_{13} comes from nozzle #1, from nozzle #3, or as result of their interaction (i.e. populations p-i, p-ii and p-iii described earlier). In order to determine the agglomerates formed only by one of the sprays, one needs to operate this nozzle alone but under the same air flow field observed when both are together in M_{13}. In essence, the solids must face the same air conditions in terms of temperature T_A, relative humidity, rH_A, and velocity, U_A in order to originate the same rate and type of particle contacts, particularly in the nozzle region. The changes introduced to replicate the air flow field observed in M_{13} during the isolation experiments are explained below; Table 2 summarizes the process conditions.

Experiments M_1, $M_{3\text{-ii}}$ and $M_{3\text{-iii}}$ replicate the air flow field in the chamber using only one slurry nozzle but matching the overall evaporation rate to that of the reference M_{13}. To do so they replace the water removed from the slurry in M_{13} with the equivalent amount provided by two sets of air/water dual nozzles (Fig. 5):

Please cite this article as: V. Francia, et al., Agglomeration in counter-current spray drying towers. Part B: Interaction between multiple spraying levels, Powder Technol. (2016), http://dx.doi.org/10.1016/j.powtec.2016.05.010

- **M_1 :** During M_{13} the flow to nozzle #3 is disconnected and the water previously evaporated from that slurry flow is injected as a fine mist by W_2, placed at the centre and facing down (Fig. 5). As shown later this allows retaining a comparable temperature field and heat transfer rate q in the top region. The product exiting the tower under these conditions represents what would have been generated by nozzle #1 in M_{13} if nozzle #3 were absent.

- **$M_{3\text{-ii}}$, $M_{3\text{-iii}}$:** In a similar way, in these cases the flow to nozzle #1 is disconnected and W_1 and W_3 are connected to maintain the same evaporation rate. Cases $M_{3\text{-ii}}$ and $M_{3\text{-iii}}$ use a different water injection ratio between W_1 and W_3 (Table 2). Two considerations must be made in respect to the use of water:
  - o Water dries faster than slurry, and thus the evaporation of droplets from W_1 and W_3 does not extend as far into the bottom of the dryer when compared to the behaviour of slurry droplets in M_{13}. As a result, the air is likely to reach a higher temperature T_A at the bottom and enhance drying. Indeed, Table 2 and later sections show that the powder in $M_{3\text{-ii}}$ and $M_{3\text{-iii}}$ reaches a higher exit temperature T_p and a lower water content X_w. This is not an issue to study agglomeration because the contacts responsible occur above, i.e. in the cylinder.
  - o Re-wetting: there is a risk for the surface of particles to be re-wet by water drops and become stickier for a short period of time. Later Section 3.3 show that some deposits appear near the water sprays despite the dual nozzles provide very fine drops (<100 μm), which are expected to dry rapidly.

Later Section 3.2 shows that during M_{13} the air temperature T_A varies from ~300 °C at the inlet to ~100 °C above nozzle #3. The same range of variation has also been controlled by modifying the inlet air conditions:

- **M_3** uses the same inlet air mass rate M_A but reduces the inlet temperature $T_{A,IN}$ until the T_A above nozzle #3 reaches the value in the reference M_{13} (~100 °C). Therefore, the same rate of heat is exchanged and the product is dried to the same water content X_w, but in turn, the air at the top of the chamber reaches higher temperatures and velocities.

- **$M_{3\text{-i}}$** keeps on reducing $T_{A,IN}$ further until the exhaust conditions match those in the reference M_{13}. Of course, this reduces the overall drying rate versus the one in M_3 and the product exits with a higher water content X_w.

Table 3 illustrates the effect of the different operating conditions in the air velocity U_A in the chamber, by the estimation of the air superficial velocity U_{av} at different levels according to the changes in air temperature given in later Section 3.2. This enables the comparison of the exhaust velocities for different cases and explain how the stronger drag causes more elutriation and presumably a higher particle concentrations at the bottom of the chamber.

3. Results and discussion

3.1. Capacity and efficiency

All cases with the exception of M_3 show comparable exhaust conditions (Tables 2 and 3, level tt-4). However, the elutriation rate M_E in Table 2 decreases when the nozzle is brought down from M_1 to $M_{3\text{-i}}$ from $M_E = 8.0\%$ of the full exit rate of powder M_{EP} to ~ 6.8% in $M_{3\text{-i}}$. The trend is in agreement with the observation made in Part A: a lower nozzle position allows more time for the elutriated powder to migrate to the walls. The operation of a multi-level arrangement results more elutriation ($M_E = 6.8-8.0\%$ vs $M_E = 2.0-4.0\%$ for single-level cases [49]) because the chamber operates at higher velocities and the air carries more solids upwards (in single-level operation conditions [49] the air mass rate and temperature are lower: $M_A/M_{A,M_{13}}$~0.67; $T_{A,IN,M_{13}} - T_{A,IN} \sim 30$ °C). When water nozzles are used in $M_{3\text{-ii}}$ and $M_{3\text{-iii}}$ the elutriation falls further perhaps as a consequence of interaction with the water drops.

When both slurry nozzles are operated together in M_{13}, the elutriation M_E represents only 3.1 % of the overall exit rate of powder M_{EP} but, remarkably, when both operate individually the summation of the elutriation rates represents 7.4% (computed from the rate of each nozzle in M_{13} and the elutriation in M_1 and $M_{3\text{-i}}$, Table 2). This is a very relevant fact: a quite substantial part of production ~4.3% flows up when both nozzles are operated independently in M_1 and $M_{3\text{-i}}$ but it no longer exits from the top if they are operated together: instead it exits at the

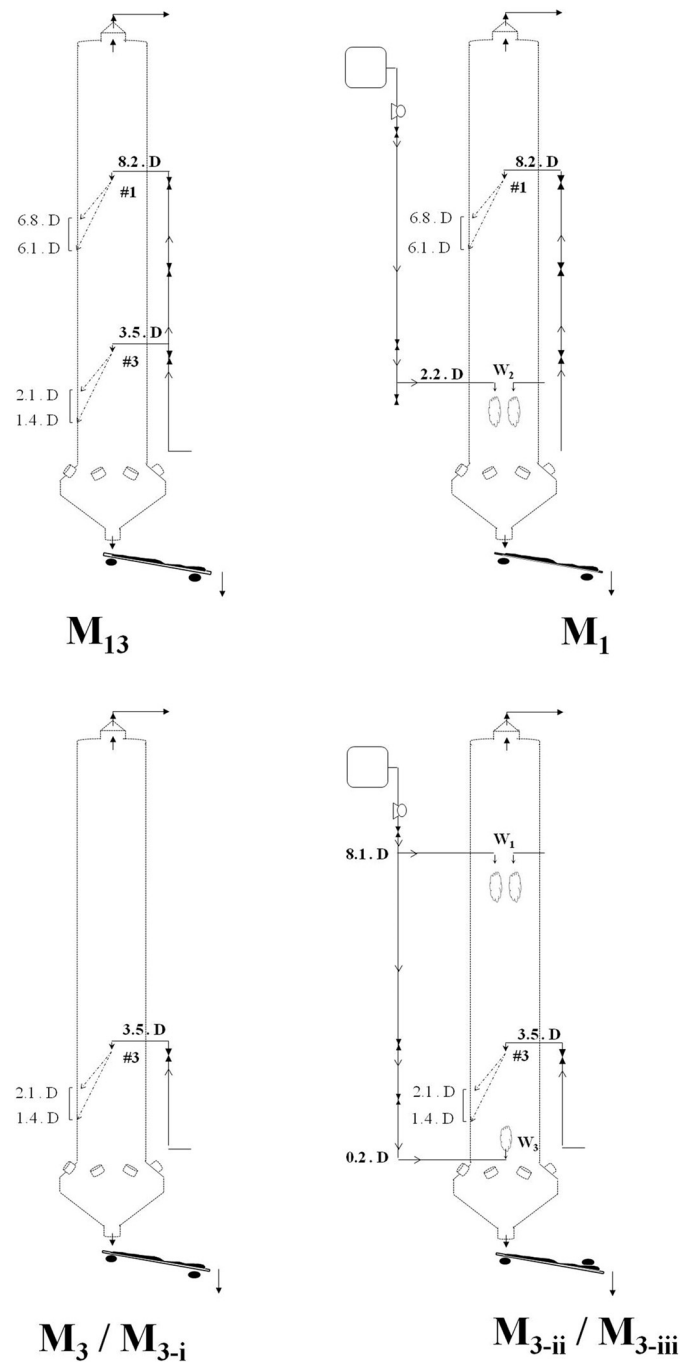

Fig. 5. Outline of experiments. A multi-nozzle reference operation denoted M_{13} plus the isolation of each of the sprays with the use of water to control the air conditions (M_1, $M_{3\text{-ii}}$ and $M_{3\text{-iii}}$) and the modification of the inlet air temperature $T_{A,IN}$ (M_3 and $M_{3\text{-i}}$).

Please cite this article as: V. Francia, et al., Agglomeration in counter-current spray drying towers. Part B: Interaction between multiple spraying levels, Powder Technol. (2016), http://dx.doi.org/10.1016/j.powtec.2016.05.010

Table 2
Operation conditions. Both spraying levels in M_{13} and the isolation of each by: a ramp in the inlet air temperature $T_{A,IN}$ (M_3, $M_{3\text{-i}}$) and the use of water sprays to replicate the evaporation rate in (M_1, $M_{3\text{-ii}}$, $M_{3\text{-iii}}$).

Scenario		M_{13}	M_1	M_3	$M_{3\text{-i}}$	$M_{3\text{-ii}}$	$M_{3\text{-iii}}$
Air phase							
$M_A/M_{A,M_{13}}$		1.00 ± 0.06	0.98 ± 0.06	1.00 ± 0.02	1.00 ± 0.02	1.00 ± 0.02	0.99 ± 0.04
$tt-0,\ T_{A,IN}$	(°C)	300.1 ± 7.0	300.7 ± 5.2	238.9 ± 2.6	169.8 ± 1.8	299.8 ± 3.2	301.5 ± 1.2
$tt-5,\ T_{A,EX}$	(°C)	78.2 ± 2.2	82.8 ± 1.6	104.8 ± 2.2	82.5 ± 1.0	75.5 ± 4.2	68.7 ± 10.4
[1]$M_{eva}/M_{eva,M_{13}}$		1.00	1.00	0.52	0.46	1.06	1.09
$rH_{A,EX}$	(%)	29	24	6	12	35	48
Particulate phase							
Nozzle(s)		#1, #3	#1, W_2	#3	#3	#1, W_1, W_3	#1, W_1, W_3
$M_{S,\#1}/M_{S,M_{13}}$		0.47 ± 0.02	0.52 ± 0.02	–	–	–	–
$M_{S,\#3}/M_{S,M_{13}}$		0.53 ± 0.02	–	0.52 ± 0.02	0.52 ± 0.02	0.53 ± 0.02	0.56 ± 0.02
[2]$M_{W_1}/\Delta M_{W,eq}$		–	–	–	–	0.36	0.58
[2]$M_{W_2}/\Delta M_{W,eq}$		–	0.98	–	–	–	–
[2]$M_{W_3}/\Delta M_{W,eq}$		–	–	–	–	0.72	0.58
$X_w - X_{w,M_{13}}$	(%)	0.00	-0.5	-0.6	4.2	-2.0	-1.6
$T_P - T_S$	(°C)	2.8 ± 3.7	1.6 ± 5.2	46.7 ± 8.1	−14.1 ± 2.2	47.0 ± 14.1	57.6 ± 9.4
M_E	(%M_{EP})	3.1	8.0	9.0	6.8	5.2	1.8
M_R	(%M_{EP})	11.6	16.1	12.7	16.4	4.6	11.3
C		0.853	0.759	0.782	0.768	0.901	0.871
Overall Energy Balance							
Q_{Loss}	(% Q_{Ex})	30.2 ± 1.8	28.0 ± 0.5	36.4 ± 0.9	19.6 ± 1.9	24.9 ± 0.7	24.5 ± 0.7
$\Delta H_{P,sn}$	(% Q_{Ex})	2.2 ± 2.7	2.2 ± 0.7	6.0 ± 1.5	−1.9 ± 2.3	4.1 ± 1.0	5.0 ± 1.0
[3]η_t		0.79 ± 0.02	0.78 ± 0.01	0.61 ± 0.01	0.58 ± 0.01	0.80 ± 0.01	0.83 ± 0.02
[4]η_h		0.57 ± 0.02	0.57 ± 0.01	0.41 ± 0.01	0.47 ± 0.02	0.62 ± 0.01	0.64 ± 0.01

A: air, IN: inlet, EX: exhaust. S: slurry, P: powder at the exit belt, E: powder at the cyclones, R: powder removed as oversized, EP: full rate of spray dried powder.
[1]*Evaporation rate* M_{eva}; [2]*Equivalent water rate* $\Delta M_{w,eq}$ *estimated from the variation in rate from single-nozzle operation to* M_{13}.[3] *Thermal efficiency* $\eta_t = (T_{A,IN} - T_{A,EX})/(T_{A,IN} - T_{amb})$; [4] *Heat transfer efficiency* $\eta_h = Q_S/H_{A,IN}$ *where* $H_{A,IN}$ *denotes inlet air enthalpy with ambient as reference.*

bottom. The lack of elutriates in M_{13} points to the agglomeration of fine powder flowing up from the bottom and somehow captured. The analysis of the product size and composition given in later sections provides further evidence.

The capacity of the dryer is affected by the amount of product that must be discarded, which comprises of the powder elutriated and collected in the cyclones, M_E, and the fraction of the product considered too coarse, denoted M_R (e.g. computed here as the fraction $x_p > 1800\ \mu m$). Table 2 includes the capacity ratio C, computed as the usable fraction of the overall exit rate of powder, M_{EP}. C decreases from a maximum of 0.92 in the single-level operation conditions [49] to 0.85 in a multi-level operation because more elutriates are generated and coarser granules start to form. However, the multi-level system still results in a more economical arrangement because it doubles the throughput and increases the thermal η_t and the heat transfer η_h efficiencies from 0.74 and 0.51 in a single-level operation [49] to 0.79 and 0.57 in M_{13} thanks to the higher ΔT driven between the phases and presumably, a longer residence time.

3.2. Control of the drying environment in the chamber

In order to compare the reference production M_{13} with those from the top or bottom levels it is important to ensure that the slurry nozzles #1 and #3 face a similar temperature field and drying rate. Fig. 6 reports the air temperature T_A in the cylindrical chamber giving time-averaged measurements at different radial and axial positions. Fig. 7 includes a cross-sectional average $T_{A,av}$ and measurements at the plenum tt-p and the conical section t-c.

The multi-level production M_{13} and that from the top nozzle in M_1 show comparable temperatures below the top slurry spray (see tt-3 in Fig. 6): a constant small bias, ~10 °C and an increase at the centre of the cylinder. In the studies of the bottom slurry nozzle, the level tt-1 shows the temperature immediately below the projection the spray. The experiments using added water, $M_{3\text{-ii}}$ and $M_{3\text{-iii}}$, render slightly lower temperatures than the reference M_{13}. In the outer region, T_A varies from 175-180 °C to 150-175 °C and 160-180 °C from having both slurry nozzles in M_{13} or only the bottom in $M_{3\text{-ii}}$ and $M_{3\text{-iii}}$ (Fig. 6). In these cases, the central region of high T_A is lost above the level of the nozzle (tt-2, Fig. 6), but it reappears at the top of the chamber (tt-3, tt-4 Fig. 6). The reason for this behaviour remains unclear but it may be related to the recirculation areas caused by the swirl, at least in isothermal flows [52]. The experiments M_3 and $M_{3\text{-i}}$ use also the bottom slurry spray but neither slurry nor water are injected at the top of the dryer. Above the nozzle (tt-2 to tt-4, Figs. 6 and 7) the entire chamber achieves a homogeneous T_A, which indicates that the elutriated powder dries rapidly near the nozzle. Below the bottom spray (tt-1) M_3 and the multi-nozzle production in M_{13} face a very similar air temperature: T_A decreases towards the wall in an indication of a higher concentration of solids and it shows a span from 185-200 ºC (M_3 Fig. 6). In turn, when the inlet air temperature $T_{A,IN}$ decreases further in the case $M_{3\text{-i}}$ the temperature faced by the solids in the nozzle region (tt-1) reduces significantly to 135-145 °C ($M_{3\text{-i}}$ Fig. 6).

A distributed energy balance is reported in Tables 4 and 5 (Sections I to V are defined in Fig. 7a). The evaporation rate M_{eva} and the heat loss rate Q_{Loss}, are obtained from overall mass and energy balances. Eq. (1) defines the overall heat exchange rate Q_{Ex} from the variation of sensible enthalpy in the dry air, $\Delta H_{DA,sn}$, and the product, $\Delta H_{P,sn}$ (i.e. inlet slurry and outlet powder, elutriation and vapour) utilised in evaporation

Table 3
Axial variation of the air superficial velocity U_{av}, estimated as $U_{av} = M_{DA}/\rho_{DA}\pi R^2$.

$U_{av}/U_{av,M_{13,tt-0}}$	M_{13}	M_1	M_3	$M_{3\text{-i}}$	$M_{3\text{-ii}}$	$M_{3\text{-iii}}$
tt-0, 0.0 D	1.00	0.98	0.89	0.77	1.00	0.99
tt-1, 0.7 D	0.78	0.77	0.80	0.71	0.75	0.76
tt-2, 3.6 D	0.66	0.67	0.66	0.62	0.65	0.63
tt-3, 6.0 D	0.64	0.65	0.66	0.62	0.64	0.63
tt-4, 9.5 D	0.61	0.61	0.66	0.61	0.61	0.60

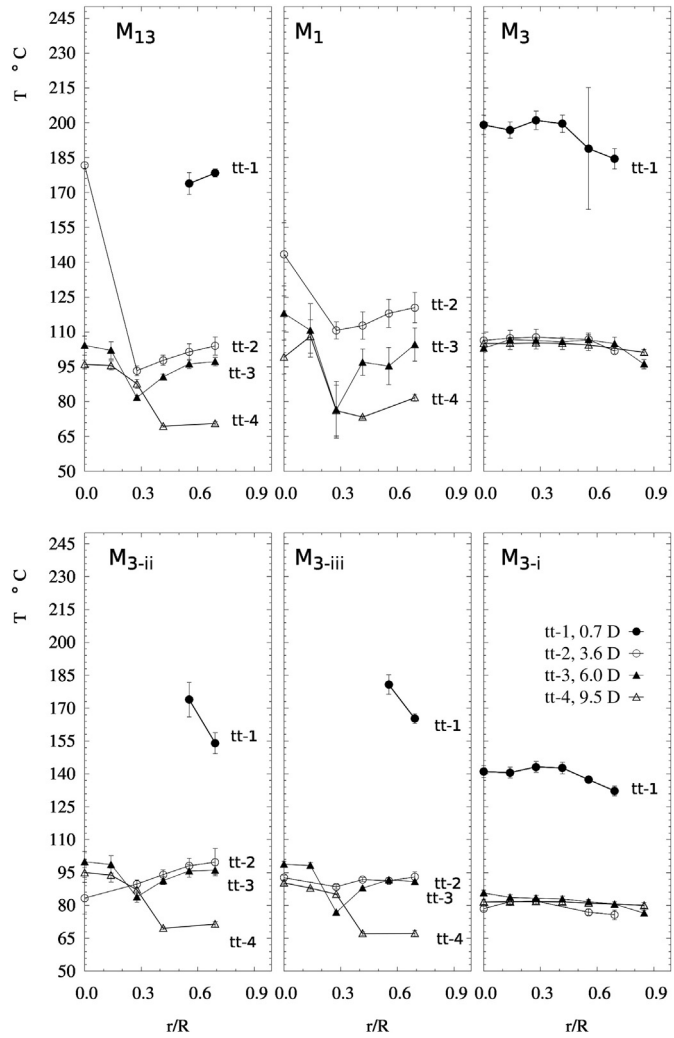

Fig. 6. Time averaged air temperature T_A in the cylindrical chamber. Radial profiles at levels tt-1 ($z = 0.7\ D$), tt-2 ($z = 3.6\ D$), tt-3 ($z = 6.0\ D$)and tt-4 ($z = 9.5\ D$). r/R denotes the normalised radial position. The top nozzle region *NR* #1 extends from 6.1-8.2 *D*; the bottom nozzle region *NR* #3 extends from1.4-3.5 *D*.

Q_{Lat}, and losses Q_{Loss}

$$Q_{Ex} = Q_{Lat} + Q_{Loss} = -(\Delta H_{DA,sn} + \Delta H_{P,sn}) \quad (1)$$

In order to study how the solids dry at different sections, it is useful to group the terms differently in Eq. (2) and compute the heat transferred to the solid phase in each section *i*, denoted $Q_{S,i}$.

$$Q_{S,i} = -(\Delta H_{DA,sn,i} + Q_{Loss,i}) = Q_{Lat,i} + \Delta H_{P,sn,i} \quad (2)$$

Eq. (2) requires the estimation of the axial distribution of the heat losses. Losses are largely localised to Section I in Fig. 7 i.e. $Q_{Loss,I} > 0.84$-$0.91\ Q_{Loss}$, and particularly, to the distributor i.e. ΔT between tt-0 and tt-p, which accounts for 0.72-0.87 Q_{Loss}. The remaining losses reduce drastically in cylinder and can be distributed according to the contact area and the air-wall temperature differences, in the assumption that all sections show comparable heat transfer resistances. In general, the energy required to heat the solids is low i.e. $\Delta H_{P,sn} < 0.10\ Q_{Ex}$, and so the heat transfer rate calculated from Q_S serves as a valid indication of the drying rate experienced by the solids.

Table 4 summarizes the axial distribution of Q_S in the reference case, M_{13}. Notably, a high proportion of heat is transferred below the cylinder >44% and a low proportion between the nozzles, Section III. There is also a large difference between both nozzle regions, Sections II and IV. Clearly, most of the particles sprayed at the top are in fact dried below the bottom nozzle in Sections I and II. To illustrate the differences, Tables 4 and 5 include a specific heat transfer rate q (*kJ* per *m* of tower and *kg* of dry slurry). Normalization by the either total rate and that of each nozzle facilitates comparison of each nozzle region in Table 5. q is indicative of the efficiency of the heat transfer and the particle concentration. For instance, in M_{13} much lower values are obtained at the top nozzle region i.e. 16.5 kJ/mkg_{DS} than the bottom nozzle region i.e. 70.6 kJ/mkg_{DS} because each faces a different drying environment. The bottom nozzle is located in areas of higher temperature, which promotes the heat transfer, and faces a stronger upwards air velocity, which must concentrates the powder further and increase the overall heat transfer rate q unless the concentration rises sufficiently to affect the temperature or cause a local mass transfer limitation.

All experiments aim at reproducing similar concentration and particle properties in the nozzle regions, and thus they must present a comparable T_A field in Fig. 7, and comparable heat transfer rates in Tables 4 and 5. The production from the top spray alone in M_1 renders an overall similar heat transfer rate to M_{13}, yet a slightly lower values at the top nozzle region, Section IV, comparing $q = 35.1$ in Table 4 (1) to 29.3 kJ/mkg_{DS} in Table 5.

The production from the bottom spray in M_3 renders higher rates i.e. 161.9 $kJ/m\ kg_{DS}$) in the nozzle region, Section II, than the reference M_{13} in Table 4 (3) i.e. 97.0-133.3 kJ/mkg_{DS}. The case $M_{3\text{-i}}$ replicates this range better using a lower inlet air temperature and yields a value of $q = 102.9\ kJ/mkg_{DS}$ in Section II. The use of the water sprays in the cases $M_{3\text{-ii}}$ and $M_{3\text{-iii}}$ renders a comparable distribution of heat exchange in the entire chamber (Table 4 (13) and Table 5). Accordingly, during M_{13} one expects the properties of the particles near the bottom nozzle, Section II, to be somewhere between those in the isolation experiments M_3 and $M_{3\text{-i}}$ without added water and $M_{3\text{-ii}}$ and $M_{3\text{-iii}}$ with added water. The first two experiments cover the range of heat transfer rate q observed in the reference, and the last two render very similar heat transfer rates but include the potential to re-wet the surface of the particles. Remarkably, all of these experiments result in a very similar product size distribution (Section 3.4) which ensures that any potential rewetting or the minor changes in the drying rate did not have significant effects in the agglomeration.

3.3. Wall deposits

During the reference M_{13}, deposits appear primarily near the projection of the top nozzle (6.9 *D*) and barely no deposits appear either between the sprays or at the bottom inspection area in 2.2 *D*. Table 6 and Fig. 8 report the initial net wall deposition rate, $r_{d,o}$, and the examination of the walls. The deposits above the nozzle respond to the accumulation of fines. In M_1 the fine droplets are directly elutriated and no deposits develop at the top (9.2 *D*), but in M_{13} heavier deposits appear despite the elutriation rate is lower (Table 2). Interestingly, more wet fine particles seem to be reaching the walls at the top and accumulate without being elutriated. It is perhaps the consequence of recirculation or wearing of deposits given the large amount of powder impacting the walls. This could explain by the deposits do in fact diminish at the top nozzle region (6.9-8.1 *D*) when comparing M_{13} to the use of the top nozzle alone in M_1.

In the projection area from nozzle #1 (6.9 *D*) the amount of deposits increase significantly from single-level operation conditions (Part A, 0.91 g/sm^2 [49]) to the use of the same nozzle under multi-level operation conditions (1.87 g/sm^2). This is a neat evidence of the effects of a two-level arrangement: the stronger counter air flow (a) increases concentration and the rate of wall impacts and (b) shifts the trajectory of coarse wet droplets upwards so that they cover more the inspection area (compare the projection between 6.1-6.8 *D* in Fig. 1 to the inspection area centred around 6.9 *D* in Fig. 2).

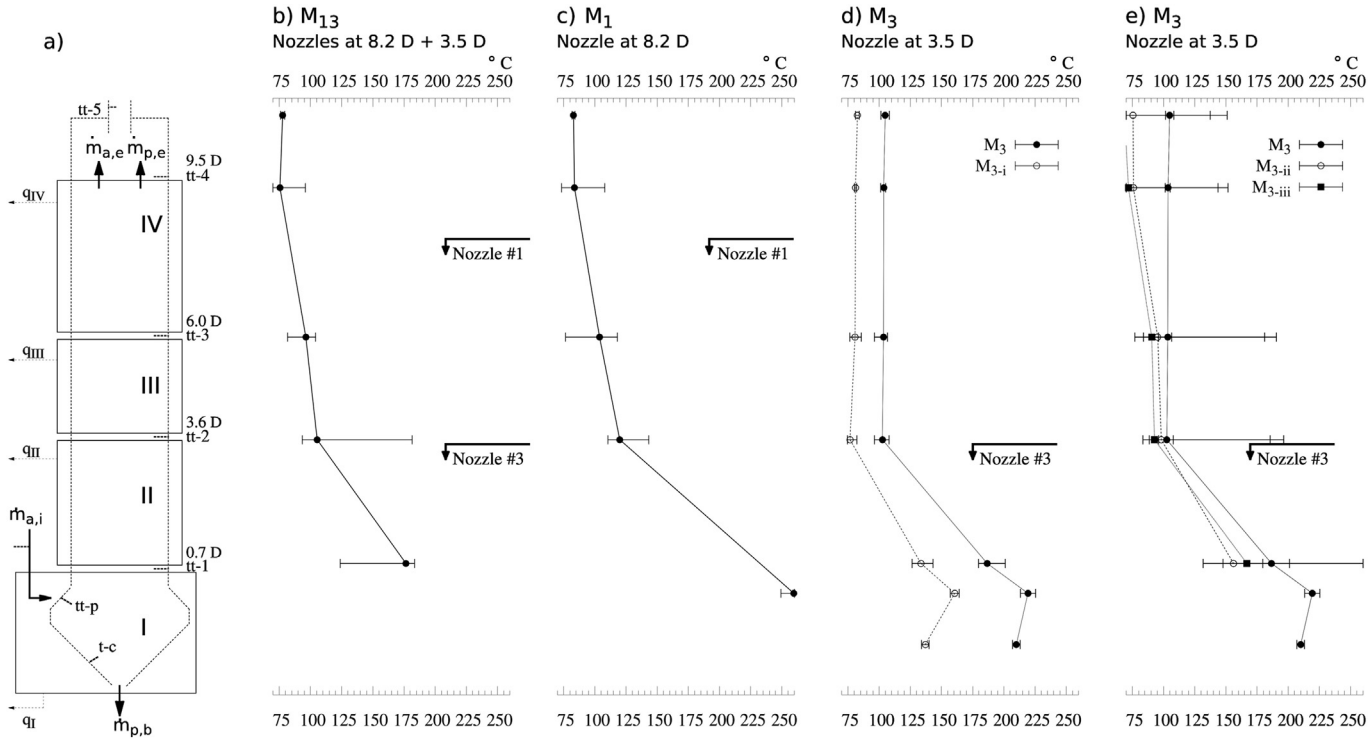

Fig. 7. Energy balance. Definition of sections I to IV (a) and axial temperature distribution. Cross sectional average $T_{A,av}$ in tt-1 to tt-4; time average in the plenum tt-p and the exhaust tt-5, and punctual measurement in the cone t-c. (b) multi-nozzle operation M_{13} from nozzle #1 ($z = 8.2\,D$) and #3 ($z = 3.5\,D$) and isolation experiments in (c) M_1: nozzle #1 and water nozzle W_2 (d) M_3 and $M_{3\text{-}i}$: nozzle #3 modifying $T_{A,IN}$ and (e) comparison of M_3 to the use of water in $M_{3\text{-}ii}$ and $M_{3\text{-}iii}$: nozzle #3 and water nozzles W_1 and W_3.

No deposits appear near the projection from nozzle #1 (2.2 *D*) in either M_{13} or the operation of the bottom nozzle in M_3 because the solids are sufficiently dry when they reach the wall. However, when the drying rate diminishes in $M_{3\text{-}i}$ the deposits start to appear, see Fig. 8b. Similarly, when added water is used in $M_{3\text{-}ii}$ and $M_{3\text{-}iii}$, some deposits start to appear near both of the water sprays (see Fig. 8b) in an indication that the surface of the particles or the walls has been re-wet. The product in these cases may contain some aggregates that would not have been produced if water drops were "invisible" to the solids, but as detailed later it poses no restrictions to the conclusions of the work

3.4. Contribution of each spray and their interaction to the agglomeration

Table 7 summarizes the statistics of all the product size distributions. Fig. 9a evidence the increase in particle size from the initial droplet population to the product in the multi-level production, M_{13}. The conditions associated to a single-level operation render product size distributions with a single mode between 300-425 *μm* [49]. The use of both sprays in M_{13} generates a clearly different bi-modal shape. The product shows the same primary mode but also a coarser second mode between 850-1180 *μm*. Fig. 9b compares the reference production M_{13} with the contribution expected from the operation of each of the nozzles independently given by M_1 and M_3. All cases show the same primary mode in Fig. 9b. The bottom spray M_3 originates a single narrow mode but the top spray, M_1 is clearly responsible of generating coarser powder and the bi-modal distribution. It is evident that agglomeration is strongly inhibited at the bottom of the dryer and promoted at the top. The reduction of the heat transfer rate observed at the top of the chamber, Table 4, makes the surface of particles in the top region wetter (either air-borne or wall-borne) and thus more prone to stick to the wall and deposit (Fig. 8) or to each other and agglomerate (Fig. 9b)

Table 4
Distributed energy balance for the multi-level production, M_{13} and specific heat transfer rates. Bold denotes the spray region(s).

Section	Multi-level system, M_{13}			
	$Q_{S,i}$	[1] q kJ/mkg_{DS}		
	%	#13	#1	#3
I $_{<0.7D}$	44.7 ±1.4		-	
II $_{0.7\text{-}3.6D}$	40.1 ±1.1	**70.6** ±0.6	150.3 ±6.5	[3]**133.3** ±5.8
III $_{3.6\text{-}6.0D}$	4.0 ±0.1	8.8 ±0.3	18.8 ±1.0	16.7 ±0.9
IV $_{6.0\text{-}9.5D}$	11.2 ±0.3	**16.5** ±0.2	[2]**35.1** ±1.5	31.1 ±1.4

[1] *Specific heat transfer rate* $q = Q_{S,i}/(\Delta z\, M_S\,(1\text{-}X_{w,S}))$; *#13, #1 or #3 denote the normalization to* M_S , $M_{S,\#1}$ *or* $M_{S,\#3}$.
[2] *Most the heat exchanged corresponds to the product from nozzle #1.*
[3] *Part of the heat is transferred to product from nozzle #1. The minimum rate transferred to the product from nozzle #3 may be estimated as* 97.0 ± 4.5 *kJ/mkg*$_{DS}$ *for a direct comparison to* M_3, $M_{3\text{-}i}$ *in Table 5.*

Table 5
Distributed energy balance and specific heat transfer rates for the isolation experiments. Bold denotes the spray region.

Section	M_1		M_3	
	$Q_{S,i}$	[1] q	$Q_{S,i}$	q
	%	kJ/mkg_{DS}	%	kJ/mkg_{DS}
I $_{<0.7D}$	81.0 ±0.1	-	13.9 ±1.6	-
II $_{0.7\text{-}3.6D}$			**86.1** ±1.6	**161.9** ±0.4
III $_{3.6\text{-}6.0D}$	8.3 ±0.1	34.3 ±0.2	0.0	0.0
IV $_{6.0\text{-}9.5D}$	**10.7** ±0.1	**29.3** ±0.1	0.0	0.0

Section	$M_{3\text{-}i}$		$M_{3\text{-}ii}$		$M_{3\text{-}iii}$	
	$Q_{S,i}$	q	$Q_{S,i}$	q	$Q_{S,i}$	q
	%	kJ/mkg_{DS}	%	kJ/mkg_{DS}	%	kJ/mkg_{DS}
I $_{<0.7D}$	29.7 ±1.8	-	57.4 ±0.4	-	50.2 ±1.4	-
II $_{0.7\text{-}3.6D}$	**70.3** ±1.8	**102.9** ±0.5	**31.5** ±0.3	**111.7** ±0.2	**39.5** ±0.4	**135.6** ±0.2
III $_{3.6\text{-}6.0D}$	0.0	0.0	0.9 ±0.1	4.0 ±0.1	0.6 ±0.1	2.6 ±0.1
IV $_{6.0\text{-}9.5D}$	0.0	0.0	10.3 ±0.1	30.4 ±0.1	9.7 ±0.1	27.6 ±0.1

[1] *specific heat transfer rate* $q = Q_{S,i} / (\Delta z\, M_S\,(1\text{-}X_{w,S}))$

Please cite this article as: V. Francia, et al., Agglomeration in counter-current spray drying towers. Part B: Interaction between multiple spraying levels, Powder Technol. (2016), http://dx.doi.org/10.1016/j.powtec.2016.05.010

Table 6
Summary of the initial deposition rates, $r_{d,o}$, at the inspection areas depicted in Figs. 2 and 8. Bold denotes the slurry projection areas.

Level	M_{13}	M_1	M_3	$M_{3\text{-i}}$	$M_{3\text{-ii}}$	$M_{3\text{-iii}}$
z / D	g/sm^2					
10.4	-	-	0.01	0.01	-	-
9.2	0.50	0.03	0	0	0	0
8.1	0.24	0.54	0	0.01	0	0
6.9	**1.37**	**1.87**	0	0.01	1.66	0.52
5.7	0	0	0	0	0	0
4.5	0	0	0	0	0	0
3.4	0	0	0	0.01	0	0
2.2	**0.06**	-	**0**	**0.68**	**1.49**	**2.25**

Table 7
Statistics of the product size distribution. Confidence intervals provide one standard deviation.

Case	$x_{p,10}$, μm	$x_{p,25}$, μm	$x_{p,50}$, μm	$x_{p,75}$, μm	$x_{p,90}$, μm
M_{13}	**163** ± 3	**246** ± 6	**423** ± 22	**1093** ± 61	**2023** ± 186
M_1	**220** ± 11	**220** ± 11	**696** ± 76	**696** ± 76	**3115** ± 1059
M_3	**175** ± 13	**237** ± 13	**334** ± 25	**697** ± 392	**3482** ± 2167
$M_{3\text{-i}}$	186 ± 10	261 ± 15	388 ± 30	1070 ± 500	4447 ± 1100
$M_{3\text{-ii}}$	175 ± 9	236 ± 13	335 ± 29	601 ± 123	2424 ± 1001
$M_{3\text{-iii}}$	179 ± 16	240 ± 17	335 ± 28	529 ± 96	1471 ± 833
S_1 [49]	**173** ± 4	**261** ± 7	**413** ± 15	**824** ± 64	**1724** ± 286
S_3 [49]	**195** ± 12	**282** ± 20	**456** ± 98	**2224** ± 1575	$x_{p,83} = 4760\ \mu m$

The comparison between the single-level and the multi-level operation conditions in Parts A and B illustrates the trade off between increasing rate and promoting particle growth. Fig. 10 compares the product obtained from nozzles #1 or #3 under multi-level operation conditions denoted M_1 and M_3 (Table 2), to single-level operation conditions, denoted S_1 and S_3 (Part A [49], $M_A/M_{A,M_{13}} \sim 0.67$, $T_{A,IN,M_{13}} - T_{A,IN} \sim 30$ °C). The production from the top nozzle #1 becomes coarser when the air mass rate increases in the multi-level case (the shoulder in S_1 develops into a second mode in M_1, Fig. 10a). The evolution can be explained by the increase in particle concentration, which multiplies the particle-particle and particle-wall contacts in the top nozzle terminal region *NTR* where the air temperature is low and the particles remain sticky. In contrast, the production from the bottom nozzle #3 becomes finer under the multi-level operation conditions (the mode in S_3 narrows in M_3 and the plateau disappear, Fig. 10b) because the higher temperature and heat transfer rate at the bottom suppress the agglomeration.

A relevant question for model development is whether the nozzles are in fact independent, i.e. whether one can assume that agglomeration occurs only between droplets/particles from the same nozzle. If the contacts due to the recirculation between both nozzles regions in Fig. 4 were negligible, the simple summation of independent productions given by $M_1 + M_3$ would result in M_{13} (or at least the maximum amount of agglomerates expected from independent sprays since M_1 and M_3 overpredict particle growth). A simple mass balance demonstrates that this is not the case. The second size mode generated in M_1 accounts as a maximum for 63% of the product $x_p > 600\ \mu m$.

Fig. 11 shows the comparison of (a) the product expected from nozzle #3 if there were no interactions between the sprays i.e. M_{13} - M_1 and

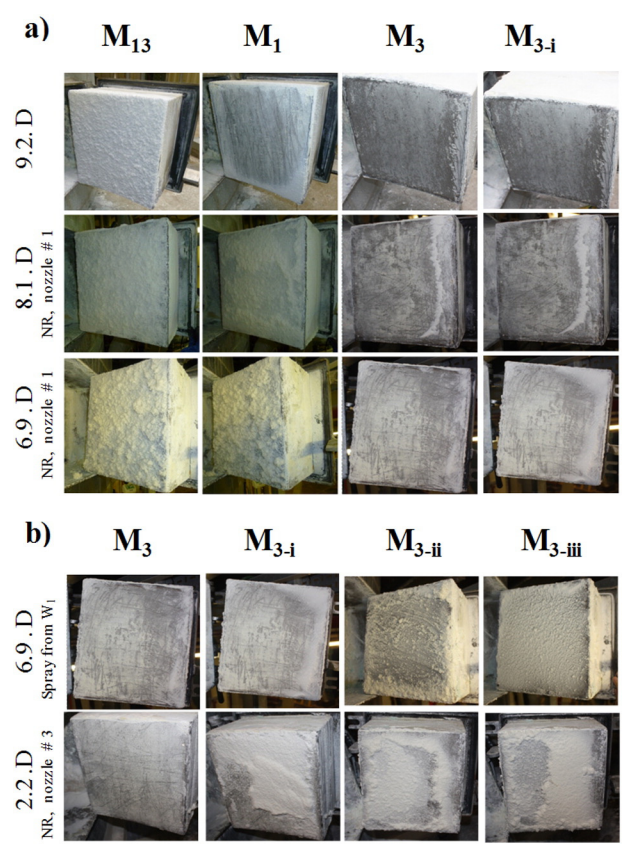

Fig. 8. Examination of the walls. (a) Deposits due to the projection of nozzle #1 and the elutriation (b) Deposits due to the projection of nozzle #3 and water dual nozzles W_1 and W_3. Areas with not significant deposits are excluded.

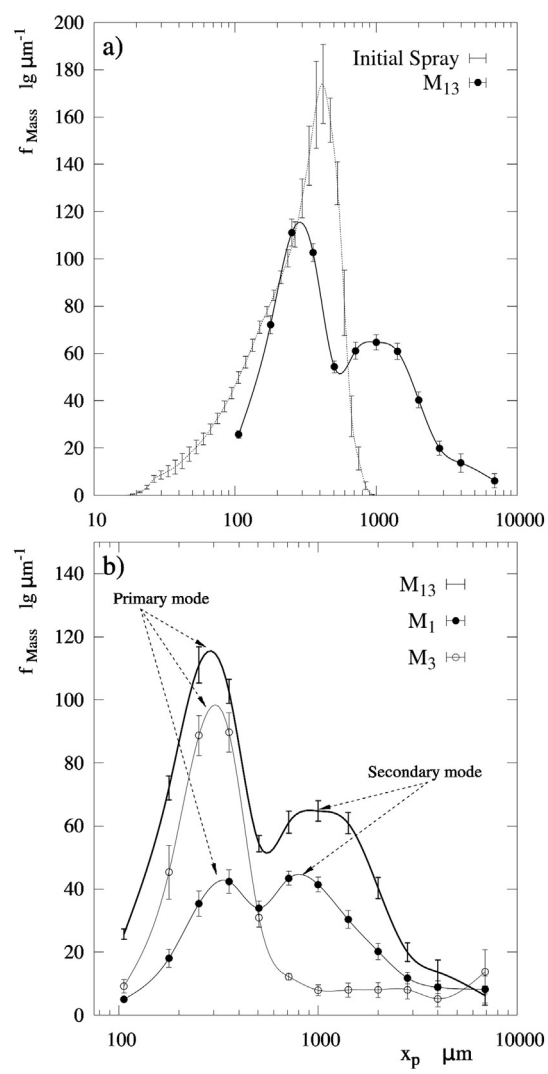

Fig. 9. Mass based product size distribution in the multi-nozzle operation M_{13}. (a) Comparison to the droplet size distribution and (b) the independent contribution from each nozzle, nozzle #1 ($z = 8.2\ D$) in M_1 and nozzle #3 ($z = 3.5\ D$) in M_3.

Please cite this article as: V. Francia, et al., Agglomeration in counter-current spray drying towers. Part B: Interaction between multiple spraying levels, Powder Technol. (2016), http://dx.doi.org/10.1016/j.powtec.2016.05.010

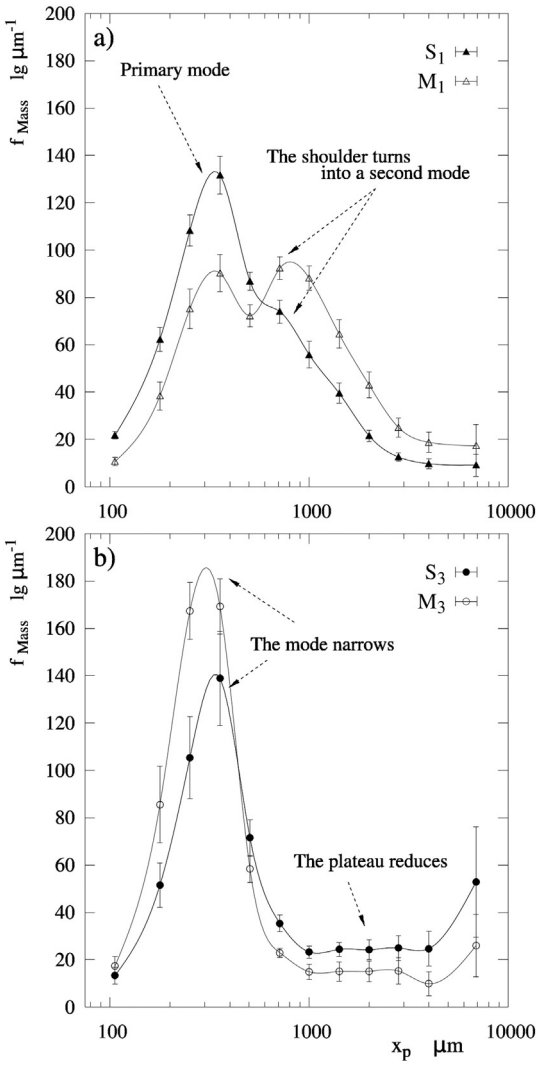

Fig. 10. Evolution of the product size distribution associated to nozzles #1 and #3 from single-level operation conditions S_1 and S_3 [49] to multi-level operation conditions M_1 and M_3 (a) nozzle #1, S_1 [49] and M_1 and (b) nozzle #3, S_3 [49] and M_3.

(b) all the experiments that isolate nozzle #3. The powder obtained from nozzle #3 always exhibits the same size distribution: a single mode aligned with the primary mode in M_{13}. The cases M_3 and $M_{3\text{-i}}$ generate narrower modes and a final plateau, instead of long tails observed when water is added in $M_{3\text{-ii}}$ and $M_{3\text{-iii}}$. When the drying rate is reduced the plateau rises in $M_{3\text{-i}}$ and a wider tail appears in $M_{3\text{-iii}}$, but in every case the shape and statistics remain very similar (Table 7). However, the product expected from independent nozzles (i.e. M_{13} - M_1) shows a clearly different distribution in Fig. 11, which demonstrates that M_{13} does not comprises of the simple summation of powder generated by top and bottom nozzles $M_1 + M_3$. Consequently, the sprays cannot be considered independent. The discrepancy in the mass balance (i.e. second mode of M_{13} - M_1 in Fig. 11) is indicative of the population of agglomerates resulting from particle contacts between different sprays. It can be estimated as the difference between the mass rate $x_p > 600$ μm in M_{13} and $M_1 + M_3$. One can state that as a minimum, 6-11% of the the secondary mode in M_{13} was generated by inter-level contacts. The inter-level agglomeration then represents 3.7% of the overall exit rate of powder, which is consistent with the reduction of the elutriation in Table 2 (quantified as 4.3%, Section 3.1). In essence, the size distributions confirm that the powder elutriated from the bottom nozzle has been entirely captured and forms part of coarser granules in M_{13}. The capture of fines and a second size mode are not found particularly detrimental to the product quality in M_{13}, for the mass median size $x_{p,50}$ remains similar to a single-level operation (S_1 or S_3 in Table 7 [49]). Furthermore, $x_{p,10}$ and $x_{p,90}$ are even reduced versus S_3 because the second mode prevents the formation of a final plateau in Fig. 9b.

Finally, the distribution of deposits at the walls is known to affect significantly the flow structure in a swirl dryer. To evaluate their effect M_{13} and M_1 were first obtained under initially clean walls and then replicated under heavily built up walls [52,53]. The product size and operation conditions result indistinguishable in all cases, which suggest that the effect of deposits in the flow remains comparable once the wall reaches an equilibrium thickness.

3.5. Product heterogeneity

3.5.1. Redistribution of active components(s) X_s

Separation of liquids and solids during the atomization makes small droplets particularly rich in liquids such as surfactant(s) and those comparable to the size of the solids suspended in the slurry (50 $\mu m < x_p < 200$ μm) particularly poor [49]. In this way, the surfactant(s) distribute preferentially into the smallest particles and the elutriated powder. Larger granules start to include more of the suspended solids and so present a minimum content in surfactant(s), and only when they grow sufficiently they render homogeneous values [49]. The

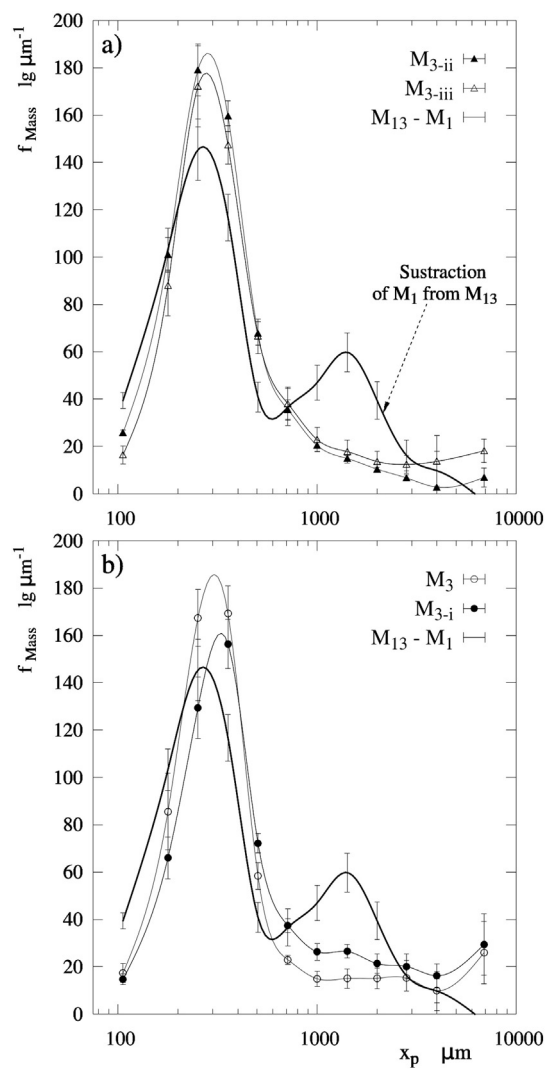

Fig. 11. Product size distribution from the bottom nozzle #3. Isolation experiments through (a) the use of water sprays in $M_{3\text{-ii}}$ and $M_{3\text{-iii}}$ and (b) modification of the inlet air temperature $T_{A,IN}$ in M_3 and $M_{3\text{-i}}$. The expectation during the multi-nozzle reference in M_{13} if both sprays were independent is given by M_{13} - M_1.

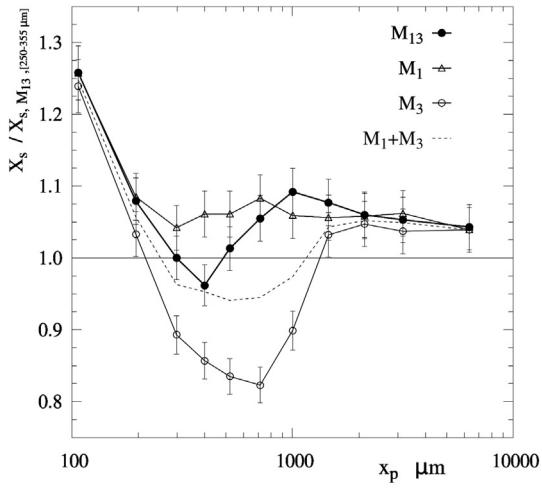

Fig. 12. Product surfactant(s) content X_s as function of particle size for the multi-nozzle operation M_{13}, and the isolation of nozzles #1 and #3, M_1 and M_3. The expectation in M_{13} if both sprays were independent is given by M_1+M_3. Data normalised to value of the mode size class in M_{13}.

experiments discussed here show the same general trend. The content of surfactant(s) in the product X_s is given in Fig. 12 comparing each size class to the primary size mode in the reference M_{13}. The effects of the phase separation are neater in the production of the bottom nozzle M_3. Since agglomeration is less significant, the smallest droplets have not yet been redistributed in coarse granules and X_s varies drastically with size. The primary size mode shows less surfactant(s) in Fig. 12 because it contains fewer agglomerates and more primary particles rich in solids than the coarsest granules. The elutriated powder and the particles $x_p < 450\ \mu m$ render the same surfactant(s) level that in a single-level operation S_3 [49] but in M_3 the low surfactant(s) affects coarser particles (up to 1180 μm) in an indication of the high rate of fines that is being elutriated (M_3 Table 2) and escaping agglomeration (see the size reduction in Fig. 10b). In a similar way to the single-level case S_3 [49] there is a neat correlation between the creation of the coarsest granules that form a plateau in the size distribution, M_3 Fig. 10b, and the homogenization of X_s in Fig. 12. In contrast, the powder from the top spray M_1, has undergone more agglomeration and the surfactant(s) have been redistributed across granules of different sizes.

When both levels are used together in M_{13}, the two mode sizes exhibit clearly different surfactant(s) contents. The first mode is mainly formed at the bottom and contains less agglomerates and the second comprises of the coarser granules formed at the top. The primary and secondary mode sizes in M_{13} show respectively ~3% lower and ~6% higher surfactant(s) levels than the same size ranges in single-level operation S_1 [49]. Fig. 12 includes a comparison between M_{13} and the expectation from the summation of independent sprays (M_1 + M_3). M_{13} shows more surfactant(s) in agglomerates between 450-600 μm in evidence of the effect of capturing the fine elutriated powder when the sprays operate together. Note in Fig. 12 that every size class in M_1+M_3 contains less surfactant(s) than M_{13}; this is a consequence of the higher rate of surfactant(s) that exits with the elutriated powder in M_1 and M_3. A mass balance, including measurements of X_s for the elutriated powder and conservative estimates of uncertainty reveals that the exit rate of surfactant(s) in the three cases in fact differs: in M_1 the exit rate of surfactant(s) is ~2% higher than in M_{13} and up to ~7% higher than in M_3 where it is below the expectation from the formula. It is a surprising and important result for it demonstrates that there must be a source of accumulation of surfactant(s) in the chamber that depends on the operation conditions (i.e. varies from M_1, M_3 and M_{13}). It can only be related to the walls. It would appear that the composition of the deposits can change in time and tend to accumulate surfactant(s). Perhaps the fragility of wall clusters is a function of X_s and those rich

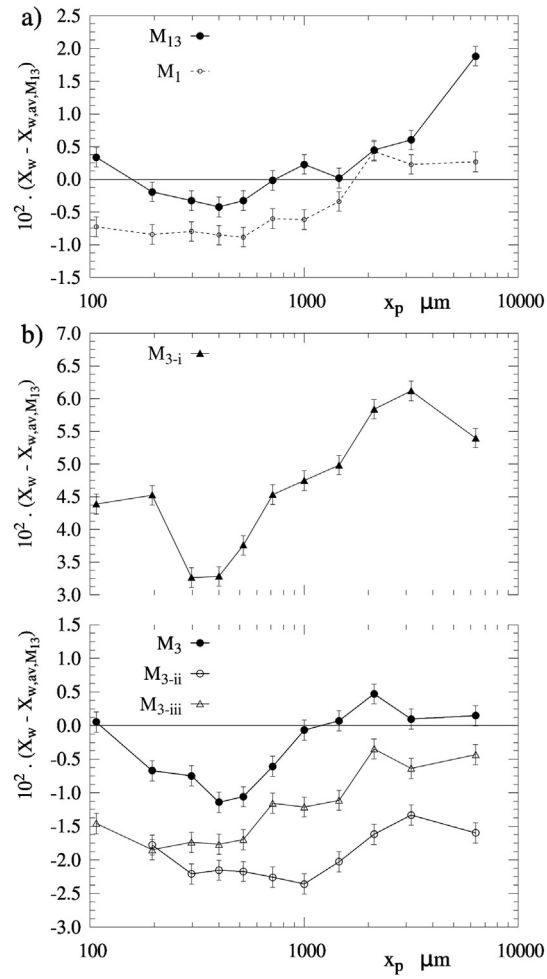

Fig. 13. Product water content X_w as function of particle size. (a) Multi-nozzle operation in M_{13} and isolation of the top spray M_1 (b) Isolation of nozzle #3 in M_3, $M_{3\text{-i}}$, $M_{3\text{-ii}}$ and $M_{3\text{-iii}}$. Difference in % in mass to the average in M_{13}.

in solids are more easily broken off and re-suspended. It is the first observation of such behaviour, which could have important effects in production and explain quality issues; this phenomenon must be studied further by long term monitoring of the deposits.

3.5.2. Particle drying history and water content, X_w

Fig. 13 includes the variation of X_w with the product particle size for M_{13} and all the isolation experiments. All cases show the general distribution as function of size characteristic of single-level operation [49]: a minimum within 350-450 μm perhaps associated to a lower initial water content, and a rise for fractions below and above, which is linked to breakage of large granules and the less efficient drying of coarse particles. It is particularly interesting that the bulk exit water content X_w is not very sensitive to the final size of the powder. X_w reduces significantly from $M_{3\text{-i}}$ to M_3, $M_{3\text{-iii}}$ and $M_{3\text{-ii}}$ in Fig. 13b but the size remains fairly constant in Fig. 11 and Table 7. This trend is inconsistent with the relation between size and drying rate when the powder settles; it may be consequence of the large proportion of drying that occurs when particles are resident at the wall, 10-100 times longer than in airborne condition [5]. Furthermore, the lack of any change in the agglomeration pattern (Fig. 11) for such a variation in water content (Fig. 13b) suggests that the growth process itself is relatively insensitive to the nature of air-borne particles (e.g. X_w) and perhaps more influenced by those at the surface of deposits (e.g. interaction of the near wall region with the walls, *NTR* and *WR* in Fig. 3). The relative importance of air-borne and wall-

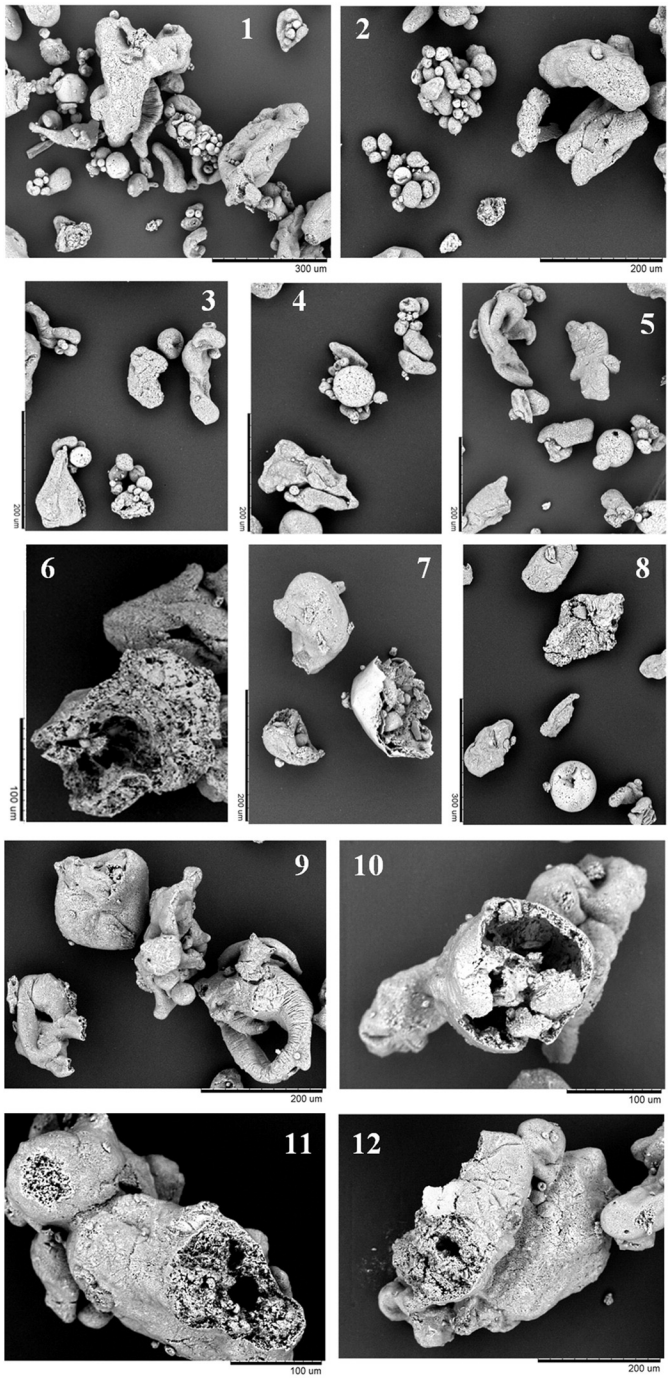

Fig. 14. Morphology of primary particles. Micrographs show elutriated powder (1 to 5), fine fractions in the product (6 to 8) and examples of coiled ligaments (9), hollow structures (10) and common porous matrix (11, 12).

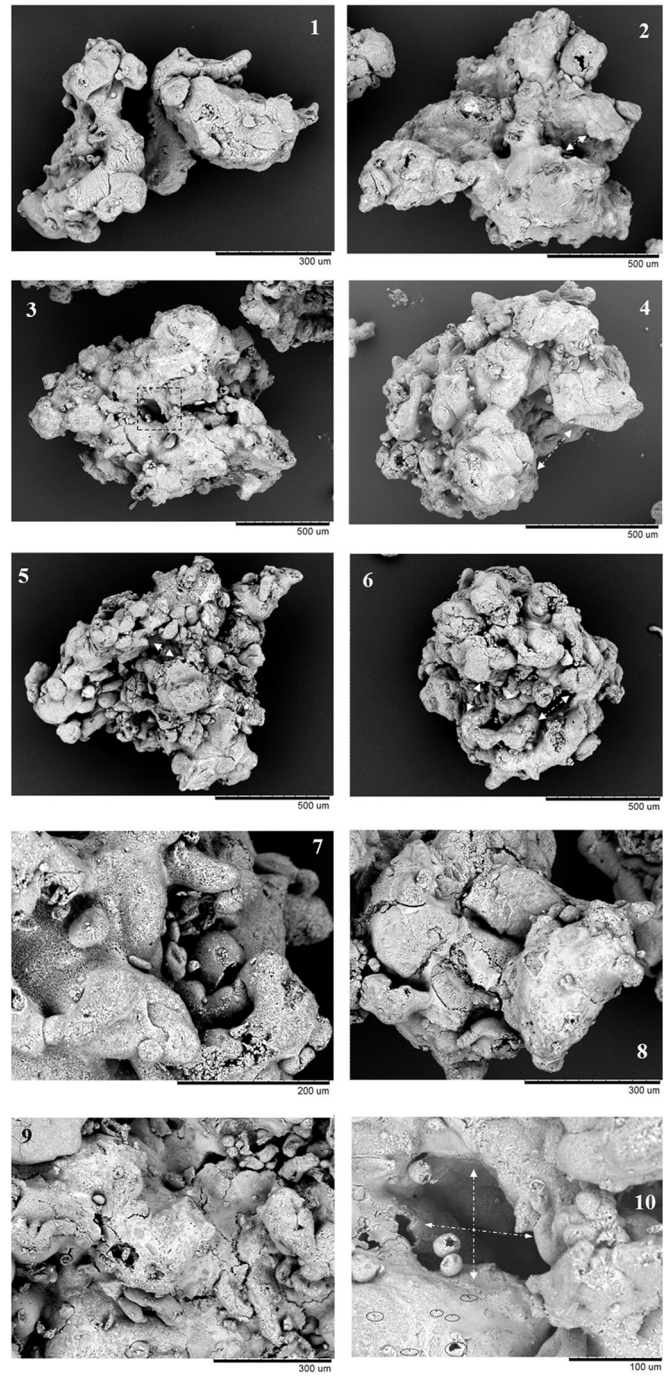

Fig. 15. Morphology of agglomerates and sources of porosity. Micrograph (1) shows fraction 355 $\mu m < x_p < 450\ \mu m$ and (2 to 6) 850 $\mu m < x_p < 1180\ \mu m$. Micrographs (7 to 10) show evidence of cracks, bursts and pores in the surface of primary particles and cavities caused by agglomeration.

borne contacts in agglomeration and drying efficiency shall be subject of future work [54].

3.5.3. Product structure

Fig. 14a shows examples of elutriated powder and fine particles to illustrate the droplet morphology (Part A [49] includes a more detailed analysis). Droplets are heterogeneous; they contain small spherical drops (e.g. Figs. 14-1 to 14-3), spherical particles of varying composition (e.g. Figs. 14-4, 14-5, 14-8) and ligaments (e.g. Fig. 14-9). Drying leads to hollow structures (Figs. 14-6, 14-10) and in vast majority a porous matrix (e.g. Figs. 14-11, 14-12). The presence of fragments (e.g. Figs. 14-6, 14-7) points to certain breakage of the coarsest granules. In general terms, a multi-level arrangement generates similar agglomerate structures and no specific morphological differences to a single nozzle [49]. Fig. 15 includes some examples and micrographs at a higher magnification to illustrate the solid bridges established between the particles and the sources of porosity due to drying or agglomeration. The agglomerates show high aspect ratios and complex shapes because they include heterogeneous primary particles and elongated shapes (e.g. Fig. 15-1). The single-level operation [49] revealed characteristic pore size ranges due to dehydration of the primary particles (micron-range) or the formation of cavities. In a multi-nozzle system the same

Table 8
Particle density and porosity for M_{13}. Bulk, envelope and skeletal densities, ρ_{bulk}, ρ_{env} and ρ_{ske}. The porosity between the envelope to the absolute or skeletal density thresholds are denoted ε_{abs} or ε_{ske}.

Size class μm	Multi-level operation, M_{13}					
	kg/m³				%	
	ρ_{bulk}	ρ_{env}	ρ_{ske}	ρ_{abs}	ε_{ske}	ε_{abs}
Elutriated	0.74	1.05 [1]	1.90	1.78	45	41
<152	0.65	0.94 [2]	1.90	1.79	51	48
152- 250	[a]	[a]	[a]	1.87	[a]	[a]
250- 355	[a]	[a]	[a]	1.93	[a]	[a]
355- 450	0.58	1.15 [3]	1.91	1.96	40	41
450- 600	0.57	1.15 [4]	1.86	1.94	38	41
600-850	0.62	1.00 [4]	1.85	1.92	46	48
850-1180	0.76	1.14 [4]	1.81	1.91	37	40
1180-1800	0.94	1.07 [4]	1.78	1.91	40	44
1800-2500	0.86	1.07 [4]	1.65	1.91	35	44
2500-4000	1.19	1.27 [4]	2.07	1.93	38	34
>4000	1.07	1.10 [4]	1.67	1.91	35	43
Average	**-**	**>1.08**	**>1.83**	**1.90**	**34-41**	**37-43**

[1,2,3,4] *refer respectively to a pore threshold size to inter-particle cavities of* 30.2, 33.0, 60.5, 90.7 *μm.*
[a] *Samples showing reproducibility issues.*

sources of porosity appear in a different size range. Fig. 15-7 to 15-10 showcase the presence of cracks, bursts and micron pores at the surface of particles and the cavities formed in the agglomerates

Table 8 reports the particle porosity ε and density as a function of size for M_{13}. Despite the different thermal history, the particle structure is found, in general terms, comparable to a single-level operation [49]. The intra-particle porosity ε shows higher values but it remains in all cases below the volume of water displaced, and no evidence suggest that droplet inflation is a dominant way to generate porosity. Fig. 16 reports the pore size distributions for selected size fractions including the entire Hg intrusion cycle (intra and inter particle voids). The product from the multi-level operation is compared to a single-level operation case with a nozzle from position #2 (intermediate between #1 and #3 [49]). When two levels are used the product coming from the top faces higher temperatures only at the bottom of the chamber when it

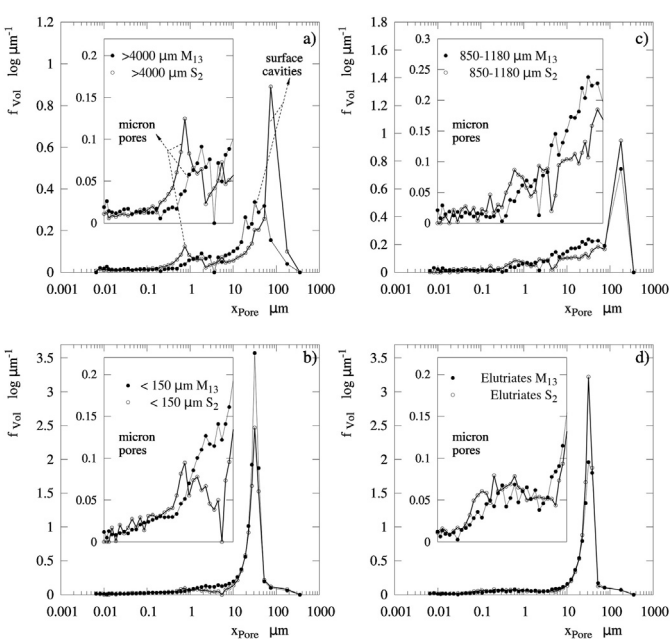

Fig. 16. Pore size distribution in the product for M_{13} and a single-level operation from an intermediate nozzle S_2 [49] (nozzle at $z = 5.9\ D$). Intrusion curves of Hg as function of particle size (a) $x_p > 4000\ \mu m$ (b) $x_p < 150\ \mu m$ (c) $850\ \mu m < x_p < 1180\ \mu m$ (d) Elutriated powder.

has already dried to some extent. In turn, the slurry sprayed at the bottom spray faces high temperature when it is still very wet and thus it is more prone to boil and generate vapour bursts. The mixture of powder from both sprays renders a more heterogeneous set of structures and makes the pore size due to drying to vary in M_{13}. The coarsest granules reveal the two sources of porosity. In the multi-level operation, M_{13}, the cavities formed by agglomeration narrow to 30-40 μm, but the micron pores move to larger sizes, perhaps as the result of bursts and faster drying rates, Fig. 16a. The same trend is observed in the finest and coarsest particles, Fig. 16a and 16b. It becomes more obscure as the agglomerates grow in Fig. 16c due to the increasing size of pores/cavities that turn comparable to inter-particle voids. In contrast, the porosity of the elutriated powder is comparable in both cases in Fig. 16d, because at the top of the dryer the fine powder experiences a similar thermal history.

4. Conclusions

The experimental method outlined here allows studying agglomeration in each spray of a large drying chamber. The effects of agglomeration in the efficiency and capacity of a multi-level swirl counter-current dryer have been investigated in an example of detergent production. The contribution of each nozzle to the product was studied independently and correlated to the process conditions and the local heat transfer rates. The following general conclusions can be summarised:

a) **Efficiency, capacity and agglomeration:** A multi-level arrangement of detergent nozzles in a swirl drying tower renders slightly lower capacity ratios than single-level operation due to the elutriation of more powder and increased agglomeration. However it allows for operation at higher throughput and improves substantially the heat transfer efficiency from 0.50 to 0.59. The different thermal history of each spray has a great impact in the formation of deposits and agglomerates. In contrast to the use of single nozzles, a two-level arrangement generates agglomerates in two size modes. The study of each nozzle independently reveals that the coarse size mode is mainly generated by the top spray. Agglomeration appears related to the specific heat transfer rate in each nozzle region: growth is heavily inhibited at the bottom and promoted at the top spray leading to creation of a coarse second size mode. In addition, the analysis of the elutriation and the powder composition demonstrates that both sprays interact by the capture of the full stream of fine powder elutriated from the bottom into the top nozzle region. In the case treated, inter-nozzle interactions account for >6-11% of agglomerates > 600 μm. The product morphology is similar for single and multiple nozzle operations but the different thermal history of the sprays makes the product in a multi-level system to present a different porosity profile and larger variations in composition due to the separation of solids and liquids phases at the nozzle.

b) **Wall dynamics:** The lack of correlation between product size and water content suggests that the contacts between particles and/or droplets occurring at the outer layers of deposits may play a substantial role in the formation of agglomerates. Furthermore, analysis of the product composition indicates that the composition of the deposits varies in time as a function of operating conditions. A relation between the resuspension dynamics and the cluster composition may be transferable to other systems and play a significant role in the long term behaviour of spray dryers, which must be studied in future works.

c) **Unit compartmentalization.** The experimental methodology described here provides a powerful tool to facilitate the development and validation of models based in the subdivision of spray dryers into nozzle regions. It enables the quantification of particle growth in different areas of a chamber and studying how

agglomeration responds to changes in process conditions. This type of data provide engineers across industries with a new way to correlate experimental growth kinetics in a specific case to the heat transfer rate near a spray, and in this way advance in developing compartmental models.

Nomenclature

A	Cross-sectional area of the cylindrical chamber, m^2
C	Capacity ratio $C = 1-((M_E + M_R)/M_{EP})$, -
D	Diameter of the cylindrical chamber, m
d	Diameter of the top exit in the dryer, tubular guard, m
erH	Equilibrium relative humidity of the product, %
f	Normalised size frequency in a probability density function, log (μm) $^{-1}$
H_A	Enthalpy rate for the air phase taking ambient temperature as a reference, J s^{-1}
$\Delta H_{DA,sn}$	Enthalpy variation between outlet and inlet air in a dry basis, J s^{-1}
$\Delta H_{P,sn}$	Enthalpy variation between the outlet product, elutriates and water vapour and the inlet slurry, J s^{-1}
M	Mass rate, kg s^{-1}
M_S	Mass rate of slurry sprayed at the nozzle, kg s^{-1}
M_E	Mass rate of powder elutriated and collected at the cyclones, kg s^{-1}
M_R	Mass rate of oversized product exiting the tower belt, kg s^{-1}
M_P	Mass rate of the product exiting the tower belt, kg s^{-1}
M_{EP}	Overall rate of powder exiting the spray drying chamber, kg s^{-1}
n	Particle number concentration, m^{-3}
Oh^2	Ohnesorge number, $Oh^2 = 2\mu_p{}^2/x_p\,\rho_p\,\sigma_p$
Q_{Lat}	Latent enthalpy rate of the water vapour generated in the chamber, J s^{-1}
Q_{Loss}	Rate of heat lost to the environment, J s^{-1}
Q_{Ex}	Rate of heat exchanged in the dryer, J s^{-1}
Q_S	Rate of heat transferred to the solid phase, J s^{-1}
q	Specific heat transfer rate per m and kg of dry slurry, kJ $m^{-1}kg_{DS}^{-1}$
$r_{d,o}$	Initial net wall deposition rate, g m^{-2} min^{-1}
rH	Relative humidity of the air, %
T	Time averaged temperature, °C
$T_{A,av}$	Cross-sectional average air temperature, $T_{A,av} = \int\rho_A U_{A,z} T_A dA/\int \rho_A U_{A,z} dA$ where normalised radial profiles for $U_{A,z}$ are taken from isothermal cases [46].
U	Time averaged velocity, m s^{-1}
U_{av}	Bulk or superficial air velocity. m s^{-1}
$U_{p,sd}$	Particle sedimentation or free falling velocity, m s^{-1}
$U_{p,t}$	Particle terminal velocity, m s^{-1}
$U_{p,w}$	Particle velocity for the first wall impact, m s^{-1}
x_p	Particle/droplet diameter, μm
x_{pore}	Pore/cavity/void diameter, μm
X_s	Product surfactant(s) mass fraction in a dry basis
X_w	Product water mass fraction.
z	Axial position in the cylindrical chamber measured from the level of the air inlets, m

Greek letters and symbols

ε_{abs}	Intra-particle porosity in pores below the envelope threshold, %
ε_{ske}	Intra-particle porosity, in pores between the envelope and skeletal thresholds, %
η_t	Thermal efficiency in the dryer, $\eta_t = (T_{A,IN} - T_{A,EX})/(T_{A,IN} - T_{amb})$
η_h	Heat transfer efficiency in the dryer, $\eta_h = Q_S / H_{A,IN}$.
μ	Slurry viscosity, kg $s^{-1}m^{-1}$
ρ	Density, kg m^{-3}
ρ_{abs}	Absolute particle density including no pores in He pycnometry, kg m^{-3}
ρ_{bulk}	Bulk particle density including cavities up to $x_{pore} < 353\ \mu m$ in Hg porosimetry, kg m^{-3}
ρ_{env}	Envelope particle density including pores smaller than the threshold in Table 8 in Hg porosimetry, kg m^{-3}
ρ_{ske}	Skeletal particle density, including pores up to $x_{pore} < 6\ nm$ in Hg porosimetry, kg m^{-3}
Ω_i	Design swirl intensity, non-dimensional flux of angular momentum [46].

Subscripts, superscripts and caps

A	For the air phase.
DA	For dry air.
DS	For dry slurry.
E	For the elutriated fraction of powder.
EP	For the full powder exiting the tower (elutriated fraction + product from the bottom)
EX	Exhaust conditions.
IN	Inlet conditions.
P	For the particle/product exiting the tower from the bottom end.
R	For the fraction of oversized powder removed from that exiting from the tower belt.
S	For surfactant(s) / for the solid phase / for the slurry mix at the nozzle.

Acknowledgments

VF was supported by an Engineering Doctorate Studentship sponsored by the Engineering and Physical Sciences Research Council (EPSRC) and Procter & Gamble in the Industrial Doctoral Centre in Formulation Engineering, School of Chemical Engineering, University of Birmingham. The authors also want to thank Mr Adrien Serout for his valuable advice in experimentation and the studies of atomization.

References

[1] K. Masters, Scale-up of spray dryers, Dry. Technol. 12 (1-2) (1995) 235–257.
[2] P.W. Appel, Modern methods of detergent manufacture, J. Surfactant Deterg. 3 (2000) 3.
[3] D.H. Huntington, The influence of the spray drying process on product properties, Dry. Technol. 22 (6) (2004) 1261–1287.
[4] G. Hassall, Wall build up in spray driers(EngD thesis) Chemical Engineering, University of Birmingham, Birmingham, United Kingdom, 2011.
[5] V. Francia, L. Martin, A.E. Bayly, M.J.H. Simmons, The role of wall deposition and re-entrainment in swirl dryers, AIChE J 61 (6) (2015) 1804–1821.
[6] D.E. Oakley, Scale-up of spray dryers with the air of computational fluid dynamics, Dry. Technol. 12 (1-2) (1994) 217–233.
[7] I.C. Kemp, D.E. Oakley, Modeling of particulate drying in theory and practice, Dry. Technol. 20 (9) (2002) 1699–1750.
[8] L. Huang, A.S. Mujumdar, Simulation of an industrial spray dryer and prediction of off-design performance, Dry. Technol. 25 (4) (2007) 703–714.
[9] M. Mezhericher, A. Levy, I. Borde, Modeling of droplet drying in spray chambers using 2D and 3D computational fluid dynamics, Dry. Technol. 27 (3) (2009) 359–370.
[10] Y. Jin, X.D. Chen, Numerical study of the drying process of different sized particles in an industrial-scale spray dryer, Dry. Technol. 27 (3) (2009) 371–381.
[11] T.A. Langrish, D.F. Fletcher, Prospects for the Modelling and Design of Spray Dryers in the 21st Century, Dry. Technol. 21 (2) (2003) 197–215.
[12] D.F. Fletcher, B. Guo, D.J.E. Harvie, J.J. Nijdam, J. Williams, What is important in the simulation of spray dryer performance and how do current CFD models perform? Appl. Math. Model. 30 (2006) 1281–1292.
[13] M.W. Woo, W.R.W. Daud, A.S. Mujumdar, S.M. Tasirin, M.Z.M. Talib, Role of rheological characteristics in amorphous food particle-wall collisions in spray drying, Powder Technol. 198 (2010) 252–257.
[14] Y. Jin, X.D. Chen, A Fundamental Model of Particle Deposition Incorporated in CFD Simulations of an In5dustrial Milk Spray Dryer Drying Technology, 28 (8) (2010) 960–971.
[15] S. Keshani, W.R.W. Daud, M.M. Nourouzi, F. Namvar, G. Mostafa, Spray drying: An overview on wall deposition, process and modelling, J. Food Eng. 146 (2015) 152–162.
[16] J. Paiva, R. Romualdo Salcedo, P. Araujo, Impact of particle agglomeration in cyclones, Chem. Eng. J. 162 (2010) 861–876.
[17] A. Alves, J. Paiva, R. Romualdo Salcedo, Cyclone optimization including particle clustering, Powder Technol. 272 (2015) 14–22.
[18] A. Gianfrancesco, C. Turchiuli, E. Dumoulin, S. Palzer, Prediction of powder stickiness along spray drying process in relation to agglomeration, Part. Sci. Technol. 27 (5) (2009) 415–427.

[19] S. Palzer, Influence of material properties on the agglomeration of water-soluble amorphous particles, Powder Technol. 189 (2009) 318–326.
[20] S. Palzer, C. Dubois, A. Gianfrancesco, Generation of Product Structures During drying of food products, Dry. Technol. 30 (1) (2012) 97–105.
[21] M. Sommerfeld, Validation of a stochastic Lagrangian modeling approach for inter-particle collisions in homogeneous isotropic turbulence, Int. J. Multiphase Flow 27 (2001) 1829–1858.
[22] R.E.M. Verdurmen, P. Menn, J. Ritzert, S. Blei, G.C.S. Nhumaio, T.S. Sørensen, M. Gunsing, J. Straatsma, M. Verschueren, M. Sibeijn, G. Schulte, U. Fritsching, K. Bauckhage, C. Tropea, M. Sommerfeld, A.P. Watkins, A.J. Yule, H. Schønfeldt, Simulation of agglomeration in spray drying installations: The EDECAD project, Dry. Technol. 22 (6) (2004) 1403–1461.
[23] B. Guo, D.F. Fletcher, T.A. Langrish, Simulation of the agglomeration in a spray using Lagrangian particle tracking, Appl. Math. Model. 28 (2004) 273–290.
[24] M. Mezhericher, A. Levy, I. Borde, Probabilistic hard-sphere model of binary particle–particle interactions in multiphase flow of spray dryers, Int. J. Multiphase Flow 43 (2012) 22–38.
[25] L. Malafronte, L. Ahrné, F. Innings, A. Jongsma, A. Rasmuson, Prediction of regions of coalescence and agglomeration along a spray dryer-Application to skim milk powder, Chem. Eng. Res. Des. 104 (2015) 703–712.
[26] C. Focke, M. Kuschel, M. Sommerfeld, D. Bothe, Collision between high and low viscosity droplets: Direct Numerical Simulations and experiments, Int. J. Multiphase Flow 56 (2013) 81–92.
[27] M. Kuschel, M. Sommerfeld, Investigation of droplet collisions for solutions with different solids content, Exp. Fluids 54 (2013) 1440.
[28] T.A. Langrish, Multi-scale mathematical modelling of spray dryers, J. Food Eng. 93 (2009) 218–228.
[29] S. Palzer, Agglomeration of pharmaceutical, detergent, chemical and food powders. Similarities and differences of materials and processes, Powder Technol. 206 (2011) 2–17.
[30] J.R. Paris, P.N. Ross, S.P. Dastur, R.L. Morris, Modeling of the Air Flow Pattern in a Counter current Spray-Drying Tower, Ind. Eng. Chem. Process. Des. Dev. 10 (2) (1971) 157–164.
[31] Davis, R.P.; Haines, M.S. and Sagel, J.A. 1971. Multilevel Spray-Drying Apparatus. US Patent 3629951. December 28 1971, The Procter & Gamble Company. Cincinnati, Ohio.
[32] Chamberlain, H.R. Production of detergent compositions by spray drying. US Patent 4963226. August 1st 1990. The Procter & Gamble Company. Cincinnati, Ohio.
[33] S. Sharma, Spray dryer simulation and air flow pattern studies(Ph.D thesis) The University of Aston, Birmingham, United Kingdom, 1990.
[34] A.E. Bayly, P. Jukes, M. Groombridge, C. McNally, Airflow Patterns in a Counter-Current Spray Drying Tower - Simulation and Measurement, International drying symposium, Sao Paulo, Part B, 22-25 2004, pp. 775–781.
[35] I. Zbiciński, L. Xuanyou, Conditions for Accurate CFD Modeling of Spray-Drying, Dry. Technol. 24 (9) (2006) 119–1114.
[36] G. Place, K. Ridgway, P.V. Danckwerts, Investigation of air-flow in a spray-drier by tracer and model techniques, Trans. IChemE 37 (1959) 269–276.
[37] V. Moshkin, A.V. Desyatov, N.P. Kakurkin, Hydrodynamic stability of the two-phase nonisothermal flow in a countercurrent spray dryer, Theor. Found. Chem. Eng. 41 (6) (2007) 816–821.
[38] P. Wawrzyniak, M. Podyma, I. Zbicinski, Z. Bartczak, J. Rabaeva, Modeling of air flow in an industrial counter-current spray drying tower, Dry. Technol. 30 (2012) 217–224.
[39] V. Francia, L. Martin, A.E. Bayly, M.J.H. Simmons, An experimental investigation of the swirling flow in a tall-form counter-current spray dryer, Exp. Thermal Fluid Sci. 65 (2015) 52–64.
[40] I. Zbicinski, Development and experimental verification of momentum, heat and mass transfer model in spray drying, Chem. Eng. J. 58 (1995) 123–133.
[41] D.J.E. Harvie, T.A.G. Langrish, D.F. Fletcher, Numerical simulations of the gas flow patterns within a tall form spray dryer, Trans. IChemE 79 (2001) 235–248.
[42] D.J.E. Harvie, T.A.G. Langrish, D.F. Fletcher, A computational fluid dynamics study of a tall-form spray dryer, Trans. IChemE C 80 (2002) 163–175.
[43] M. Ali, Numerical modelling of a counter-current spray drying tower(PhD thesis) University of Leeds, Leeds, United Kingdom, 2014.
[44] I. Zbicinski, A. Delag, C. Strumillo, J. Adamiec, Advanced experimental analysis of drying kinetics in spray drying, Chem. Eng. J. 86 (2002) 207–216.
[45] I. Zbicinski, C. Strumillo, A. Delag, Drying kinetics and particle residence time in spray drying, Dry. Technol. 20 (9) (2002) 1751–1768.
[46] I. Zbicinski, M. Piatkowski, Continuous and discrete phase behavior in counter current spray drying, Dry. Technol. 27 (12) (2009) 1353–1362.
[47] I. Zbicinski, R. Zietara, CFD model of counter-current spray drying process, Drying, São Paulo, Brazil, A 2004, pp. 169–176.
[48] G. Fieg, G. Wozny, K. Buick, L. Jeromin, Estimation of the drying rate and moisture profiles in an industrial spray dryer by means of experimental investigations and a simulation study, Chem. Eng. Technol. 17 (1994) 235–241.
[49] V. Francia, L. Martin, A.E. Bayly, M.J.H. Simmons, Agglomeration in counter-current spray drying towers, Part A: Particle interactions and the effect of the nozzle height, 2016, http://dx.doi.org/10.1016/j.powtec.2016.05.011.
[50] L. Ozmen, T.A.G. Langrish, An experimental investigation of the wall deposition of milk powder in a pilot-scale spray dryer, Dry. Technol. 21 (7) (2003) 1235–1252.
[51] K. Kota, T.A.G. Langrish, Fluxes and patterns of wall deposits for skim milk in a pilot-scale spray dryer, Dry. Technol. 24 (8) (2006) 993–1001.
[52] V. Francia, L. Martin, A.E. Bayly, M.J.H. Simmons, Influence of wall friction on flow regimes and scale up of swirl spray dryers, Chem. Eng. Sci. 134 (2015) 399–413.
[53] V. Francia, Spray drying of detergents in counter current towers: A study of turbulent swirling flows, fouling and agglomeration(EngD thesis) School of Chemical Engineering, University of Birmingham, Birmingham, UK, 2015.
[54] V. Francia, L. Martin, A.E. Bayly, M.J.H. Simmons, Particle aggregation in large counter-current spray drying towers: Nozzle configuration, vortex momentum and temperature, 7th World Congress in Particle Technology WCPT, Beijing, R.P.China, 2014, Procedia Engineering, 102 2015, pp. 668–675.

Please cite this article as: V. Francia, et al., Agglomeration in counter-current spray drying towers. Part B: Interaction between multiple spraying levels, Powder Technol. (2016), http://dx.doi.org/10.1016/j.powtec.2016.05.010